Kernforschungszentrum Karlsruhe
Institut für Neutronenphysik
und Reaktortechnik

G.Buckel, R.Froehlich
K.Küfner, B.Stehle

January 2nd, 1975

L - 167 a.

A fast reactor benchmark problem in two and three space dimensions

There is a high need for benchmark problems in order to test and to compare the performance and accuracy of computational methods and of computer codes for the solution of reactor physics problems.

In what follows such a model-problem is described which has been designed mainly for neutron-diffusion calculations. The layout shown in pictures 1.a), 1.b), 2.a), 2.b) has its origin in the MARK I core design of the SNR 300, a sodium cooled fast breeder prototypereactor. Only some modifications have been made in oder to facilitate the representation of the reactor in the computer code input.

The whole benchmark problem consists of one three-dimensional model in triangular-z-geometry (see pict. 1.a), 1.b)) and a consistent one in rectangular x-y-z-geometry (see pict. 2.a), 2.b)). For each of the two geometries two twodimensional models have been developed. Relatively big homogeneous material zones have been chosen and the energy range is divided into four groups only, so input preparation and computing time should be reasonable. Note that the control-rods are inserted to different positions (see pict. 2.b)).

Table 1 gives the detailed composition of the different mixtures used (note that the mixture numbers 5, 6, 7 are neither defined there nor used in the layout), table 2 gives alternatively macroscopic cross-sections for all energy groups (which were obtained by a standard condensation process starting from the 26 group KFKINR cross section set).

86080001

The boundary conditions are chosen in such a way that pictures 1.a) and 1.b) resp. 2.a), and 2.b) represent one sixth resp. a quarter of the whole reactor. Outer boundary conditions are logarithmic, i.e. flux equal to zero at extrapolated boundaries . Note, that due to symmetries, as shown in picture 1.a), it is possible to calculate 30, 60, 90, 120, 180 and 360 degree sectors of the full reactor. The normal case however is considered to be the 120 degree sector.

For the twodimensional models the cutting planes (z= constant) are chosen such that (see pict. 1.b) and 2.b)) in the first model some control-rod positions contain absorber material and some follower material whereas for the second model only follower material is found in control-rod positions. For twodimensional calculations the buckling factor is assumed be zero.

For a realistic comparison of computing time it is proposed to start with a constant flux guess and to choose as "convergence criteria" for k_{eff} 10^{-4} (10^{-5}) and for fluxes 10^{-3} (10^{-4}). The values in parantheses are the values for twodimensional calculations. The detailed measuring of the convergence criteria should be explained in the documentation of the results.

86080002

TAB. 1: Atomic compositions (10^{+24} at/cm^3)

Comp. 1:	CR520	$0.334470 \cdot 10^{-2}$	Comp. 2:	CR520	$0.334470 \cdot 10^{-2}$
	FE560	$0.110890 \cdot 10^{-1}$		FE560	$0.110890 \cdot 10^{-1}$
	MO960	$0.156334 \cdot 10^{-3}$		MO960	$0.156334 \cdot 10^{-3}$
	NA230	$0.103501 \cdot 10^{-1}$		NA230	$0.103501 \cdot 10^{-1}$
	NB930	$0.104014 \cdot 10^{-3}$		NB930	$0.104014 \cdot 10^{-3}$
	NI590	$0.247123 \cdot 10^{-2}$		NI590	$0.247123 \cdot 10^{-2}$
	O 160	$0.124809 \cdot 10^{-1}$		O 160	$0.125310 \cdot 10^{-1}$
	PU400	$0.305554 \cdot 10^{-3}$		PU400	$0.443006 \cdot 10^{-3}$
	PU410	$0.347220 \cdot 10^{-4}$		PU410	$0.503416 \cdot 10^{-4}$
	PU420	$0.694441 \cdot 10^{-5}$		PU420	$0.100683 \cdot 10^{-4}$
	PU9A0	$0.104166 \cdot 10^{-2}$		PU9A0	$0.151025 \cdot 10^{-2}$
	U 5A0	$0.121290 \cdot 10^{-4}$		U 5A0	$0.106296 \cdot 10^{-4}$
	U 8A0	$0.483946 \cdot 10^{-2}$		U 8A0	$0.424120 \cdot 10^{-2}$
	V 510	$0.658087 \cdot 10^{-4}$		V 510	$0.658087 \cdot 10^{-4}$
Comp. 3:	CR520	$0.382146 \cdot 10^{-2}$	Comp. 4:	CR520	$0.336830 \cdot 10^{-2}$
	FE560	$0.123953 \cdot 10^{-1}$		FE560	$0.111654 \cdot 10^{-1}$
	MO960	$0.207136 \cdot 10^{-3}$		MO960	$0.157626 \cdot 10^{-3}$
	NA230	$0.699362 \cdot 10^{-2}$		NA230	$0.995783 \cdot 10^{-2}$
	NB930	$0.118841 \cdot 10^{-3}$		NB930	$0.104749 \cdot 10^{-3}$
	NI590	$0.310313 \cdot 10^{-2}$		NI590	$0.249052 \cdot 10^{-2}$
	O 160	$0.196203 \cdot 10^{-1}$		O 160	$0.138479 \cdot 10^{-1}$
	U 5A0	$0.245254 \cdot 10^{-4}$		U 5A0	$0.173099 \cdot 10^{-4}$
	U 8A0	$0.978563 \cdot 10^{-2}$		U 8A0	$0.690663 \cdot 10^{-2}$
				V 510	$0.657752 \cdot 10^{-4}$
Comp. 8:	B 100	$0.604851 \cdot 10^{-2}$	Comp. 9:	CR520	$0.260524 \cdot 10^{-2}$
	B 110	$0.247954 \cdot 10^{-1}$		FE560	$0.845038 \cdot 10^{-2}$
	C 120	$0.771097 \cdot 10^{-2}$		MO960	$0.141213 \cdot 10^{-3}$
	CR520	$0.410375 \cdot 10^{-2}$		NA230	$0.189532 \cdot 10^{-1}$
	FE560	$0.133110 \cdot 10^{-1}$		NB930	$0.810186 \cdot 10^{-4}$
	MO960	$0.222437 \cdot 10^{-3}$		NI590	$0.211552 \cdot 10^{-2}$
	NA230	$0.958653 \cdot 10^{-2}$			
	NB930	$0.127620 \cdot 10^{-3}$			
	NI590	$0.333236 \cdot 10^{-2}$			

86080003

TAB. 2: Macroscopic cross-sections for 4 energy groups

(Group constant set: KFKINR001)

Scheme of condensation in relation to 26 energy groups of ABN set:

group 1: 1,5 (10.5 - 0.8 MeV)

group 2: 6,11 (0.8 MeV- 10.0 KeV)

group 3: 12,14 (10.0 - 1.0 KeV)

group 4: 15,26 (1 KeV - therm)

Composition 1: Core, inner part

Composition 2: Core, outer part

Composition 3: radial blanket

Composition 4: axial blanket

Composition 8: absorber

Composition 9: follower

(The unusual numbering of compositions has been used because of extracting the compositions 1, 2, 3, 4, 8 and 9 out of a 17 composition cross section block)

	group 1:	group 2:	group 3:	group 4:
CHI				
M1	0.768	0.232	0.0	0.0
M2	0.768	0.232	0.0	0.0
M3	0.768	0.232	0.0	0.0
M4	0.768	0.232	0.0	0.0
M8	0.768	0.232	0.0	0.0
M9	0.768	0.232	0.0	0.0
NUSF				
M1	$0.11878 \cdot 10^{-1}$	$0.53252 \cdot 10^{-2}$	$0.10471 \cdot 10^{-1}$	$0.26611 \cdot 10^{-1}$
M2	$0.14943 \cdot 10^{-1}$	$0.76887 \cdot 10^{-2}$	$0.14809 \cdot 10^{-1}$	$0.38159 \cdot 10^{-1}$
M3	$0.77427 \cdot 10^{-2}$	$0.10825 \cdot 10^{-3}$	$0.29742 \cdot 10^{-3}$	$0.84687 \cdot 10^{-3}$
M4	$0.54279 \cdot 10^{-2}$	$0.75857 \cdot 10^{-4}$	$0.21218 \cdot 10^{-3}$	$0.57592 \cdot 10^{-3}$
M8	0.0	0.0	0.0	0.0
M9	0.0	0.0	0.0	0.0
SREM				
M1	$0.28204 \cdot 10^{-1}$	$0.52747 \cdot 10^{-2}$	$0.17612 \cdot 10^{-1}$	$0.26546 \cdot 10^{-1}$
M2	$0.28782 \cdot 10^{-1}$	$0.60491 \cdot 10^{-2}$	$0.19510 \cdot 10^{-1}$	$0.33714 \cdot 10^{-1}$
M3	$0.35959 \cdot 10^{-1}$	$0.58855 \cdot 10^{-2}$	$0.16041 \cdot 10^{-1}$	$0.13349 \cdot 10^{-1}$
M4	$0.29093 \cdot 10^{-1}$	$0.44909 \cdot 10^{-2}$	$0.13082 \cdot 10^{-1}$	$0.99562 \cdot 10^{-2}$
M8	$0.24814 \cdot 10^{-1}$	$0.16412 \cdot 10^{-1}$	$0.72122 \cdot 10^{-1}$	0.16868
M9	$0.13159 \cdot 10^{-1}$	$0.14559 \cdot 10^{-2}$	$0.46001 \cdot 10^{-2}$	$0.78660 \cdot 10^{-3}$

86080004

	group 1:	group 2:	group 3:	group 4:
SFISS				
M1	$0.39123 \cdot 10^{-2}$	$0.18286 \cdot 10^{-2}$	$0.36334 \cdot 10^{-2}$	$0.92415 \cdot 10^{-2}$
M2	$0.48531 \cdot 10^{-2}$	$0.26377 \cdot 10^{-2}$	$0.51332 \cdot 10^{-2}$	$0.13238 \cdot 10^{-1}$
M3	$0.27688 \cdot 10^{-2}$	$0.44347 \cdot 10^{-4}$	$0.12274 \cdot 10^{-3}$	$0.34952 \cdot 10^{-3}$
M4	$0.19453 \cdot 10^{-2}$	$0.31065 \cdot 10^{-4}$	$0.87566 \cdot 10^{-4}$	$0.23769 \cdot 10^{-3}$
M8	0.0	0.0	0.0	0.0
M9	0.0	0.0	0.0	0.0
STR				
M1	0.11587	0.21220	0.46137	0.34571
M2	0.11588	0.21213	0.46770	0.35349
M3	0.14584	0.28443	0.52703	0.40732
M4	0.12270	0.23133	0.46274	0.33749
M8	0.13317	0.25355	0.58044	0.54168
M9	$0.72206 \cdot 10^{-1}$	0.11487	0.32642	0.19272

SMTOT			
	1 → 2		
M1	$0.23597 \cdot 10^{-1}$		
M2	$0.23262 \cdot 10^{-1}$		
M3	$0.32071 \cdot 10^{-1}$		
M4	$0.26322 \cdot 10^{-1}$		
M8	$0.22946 \cdot 10^{-1}$		
M9	$0.12942 \cdot 10^{-1}$		
	1 → 3	2 → 3	
M1	$0.40791 \cdot 10^{-5}$	$0.16153 \cdot 10^{-2}$	
M2	$0.46451 \cdot 10^{-5}$	$0.15718 \cdot 10^{-2}$	
M3	$0.38880 \cdot 10^{-5}$	$0.27776 \cdot 10^{-2}$	
M4	$0.28907 \cdot 10^{-5}$	$0.22889 \cdot 10^{-2}$	
M8	$0.10320 \cdot 10^{-5}$	$0.37687 \cdot 10^{-2}$	
M9	$0.68780 \cdot 10^{-6}$	$0.12871 \cdot 10^{-2}$	
	1 → 4	2 → 4	3 → 4
M1	$0.44493 \cdot 10^{-7}$	$0.42309 \cdot 10^{-7}$	$0.46838 \cdot 10^{-2}$
M2	$0.49968 \cdot 10^{-7}$	$0.40724 \cdot 10^{-7}$	$0.43414 \cdot 10^{-2}$
M3	$0.45039 \cdot 10^{-7}$	$0.90018 \cdot 10^{-7}$	$0.58971 \cdot 10^{-2}$
M4	$0.33248 \cdot 10^{-7}$	$0.62133 \cdot 10^{-7}$	$0.53536 \cdot 10^{-2}$
M8	$0.10489 \cdot 10^{-7}$	$0.70361 \cdot 10^{-11}$	$0.86815 \cdot 10^{-2}$
M9	$0.69903 \cdot 10^{-8}$	$0.43633 \cdot 10^{-11}$	$0.34533 \cdot 10^{-2}$

86080005

SCAPT	group 1:	group 2:	group 3:	group 4:
M1	$0.73776 \cdot 10^{-3}$	$0.18315 \cdot 10^{-2}$	$0.93000 \cdot 10^{-2}$	$0.17323 \cdot 10^{-1}$
M2	$0.71134 \cdot 10^{-3}$	$0.18403 \cdot 10^{-2}$	$0.10041 \cdot 10^{-1}$	$0.20503 \cdot 10^{-1}$
M3	$0.11854 \cdot 10^{-2}$	$0.30639 \cdot 10^{-2}$	$0.10030 \cdot 10^{-1}$	$0.13012 \cdot 10^{-1}$
M4	$0.86927 \cdot 10^{-3}$	$0.21714 \cdot 10^{-2}$	$0.76478 \cdot 10^{-2}$	$0.97272 \cdot 10^{-2}$
M8	$0.18666 \cdot 10^{-2}$	$0.12645 \cdot 10^{-1}$	$0.63443 \cdot 10^{-1}$	0.16868
M9	$0.21684 \cdot 10^{-3}$	$0.16956 \cdot 10^{-3}$	$0.11497 \cdot 10^{-2}$	$0.78672 \cdot 10^{-3}$
1/V				
M1	$0.58026 \cdot 10^{-9}$	$0.24847 \cdot 10^{-8}$	$0.12547 \cdot 10^{-7}$	$0.31651 \cdot 10^{-7}$
M2	$0.58026 \cdot 10^{-9}$	$0.24847 \cdot 10^{-8}$	$0.12547 \cdot 10^{-7}$	$0.31651 \cdot 10^{-7}$
M3	$0.58026 \cdot 10^{-9}$	$0.24847 \cdot 10^{-8}$	$0.12547 \cdot 10^{-7}$	$0.31651 \cdot 10^{-7}$
M4	$0.58026 \cdot 10^{-9}$	$0.24847 \cdot 10^{-8}$	$0.12547 \cdot 10^{-7}$	$0.31651 \cdot 10^{-7}$
M8	$0.58026 \cdot 10^{-9}$	$0.24847 \cdot 10^{-8}$	$0.12547 \cdot 10^{-7}$	$0.31651 \cdot 10^{-7}$
M9	$0.58026 \cdot 10^{-9}$	$0.24847 \cdot 10^{-8}$	$0.12547 \cdot 10^{-7}$	$0.31651 \cdot 10^{-7}$

86080006

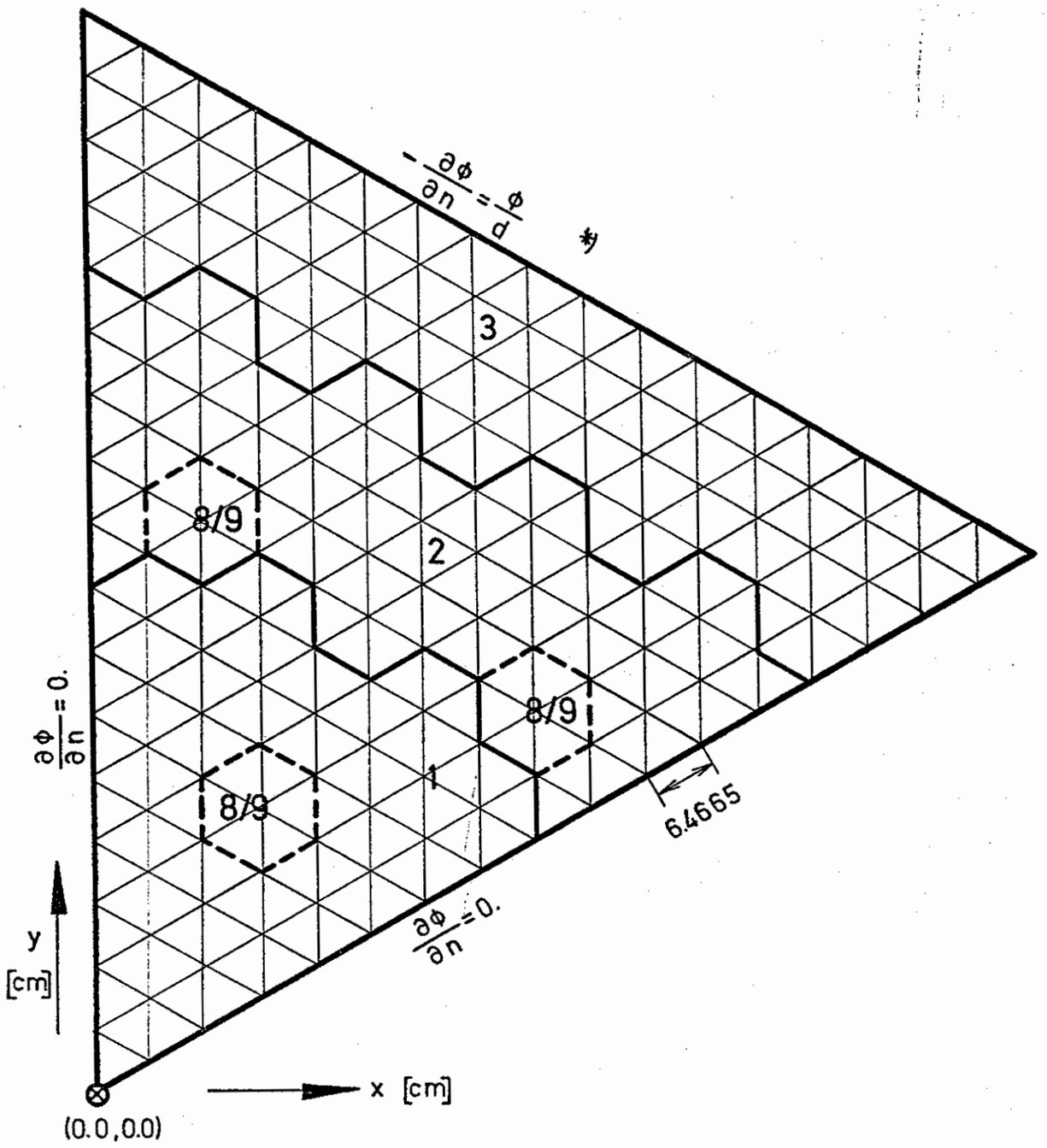

*) $d = 0.71 \cdot \lambda_{tr}$

1: Core, inner part
2: Core, outer part
3: radial blanket
4: axial blanket
8: absorber rod
9: follower

Fig. 1a): Axial section of the benchmark problem for triangular geometry

86080007

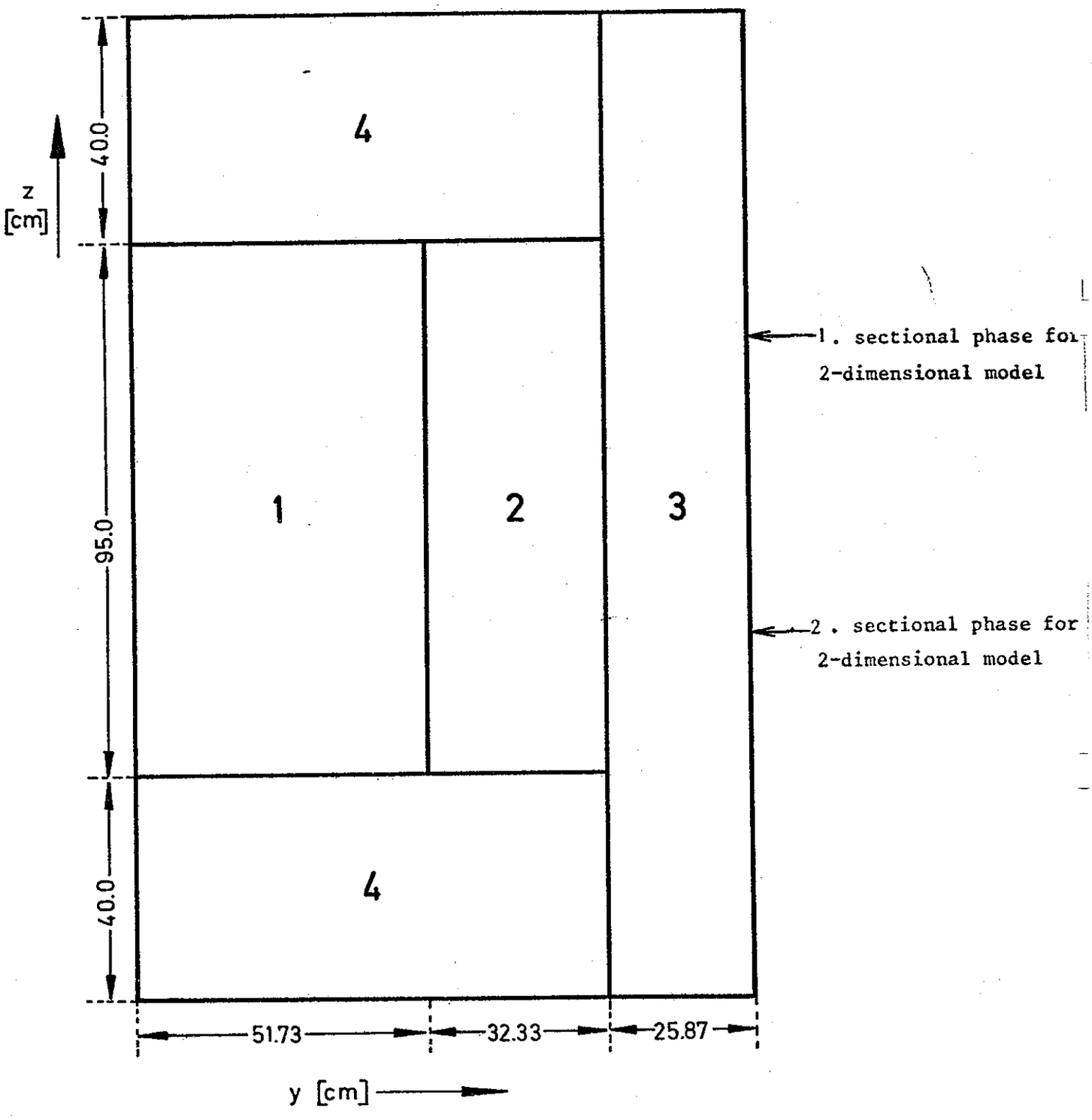

Fig. 1b): Transversal section of the benchmark problem for triangular geometry (x = y = 0.).

86080008

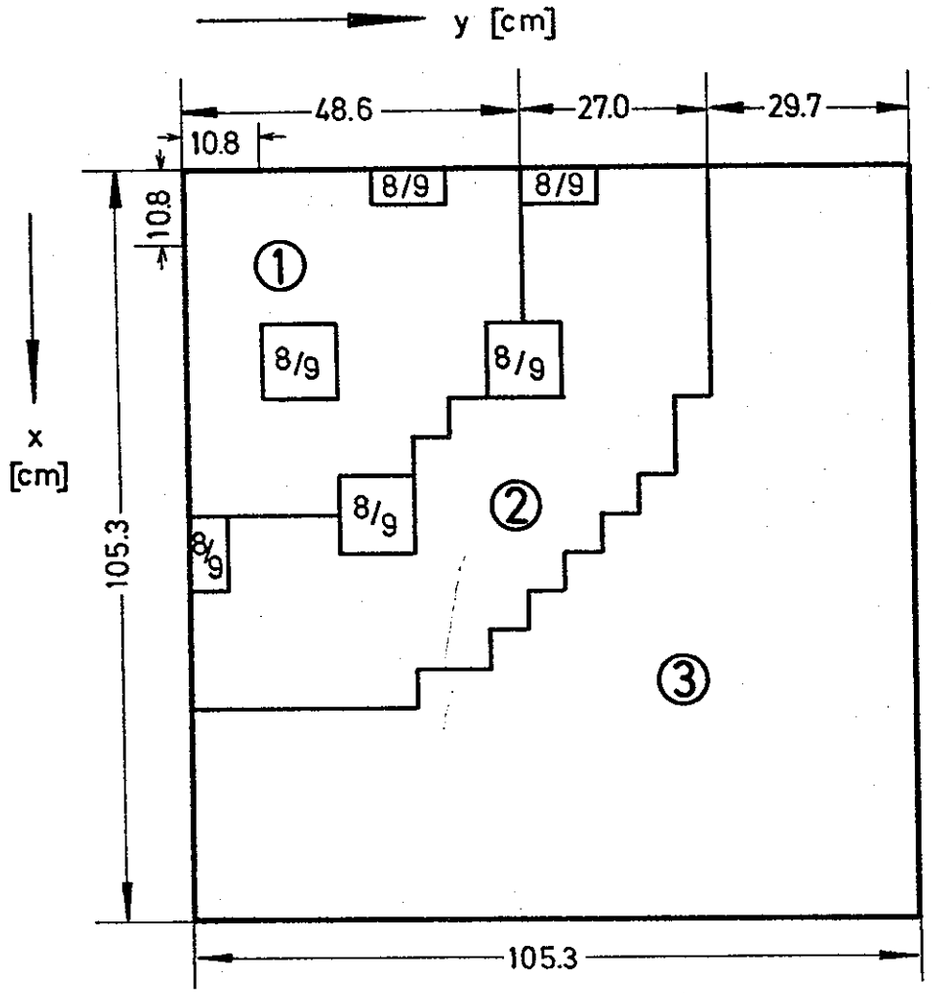

Boundary conditions:

Left and upper boundary: $\frac{\partial \phi}{\partial n} = 0.$

otherwise: $\frac{\partial \phi}{\partial n} = -\frac{\phi}{d}$

Fig. 2a): Axial section of the benchmark problem in x y z geometry

86080009

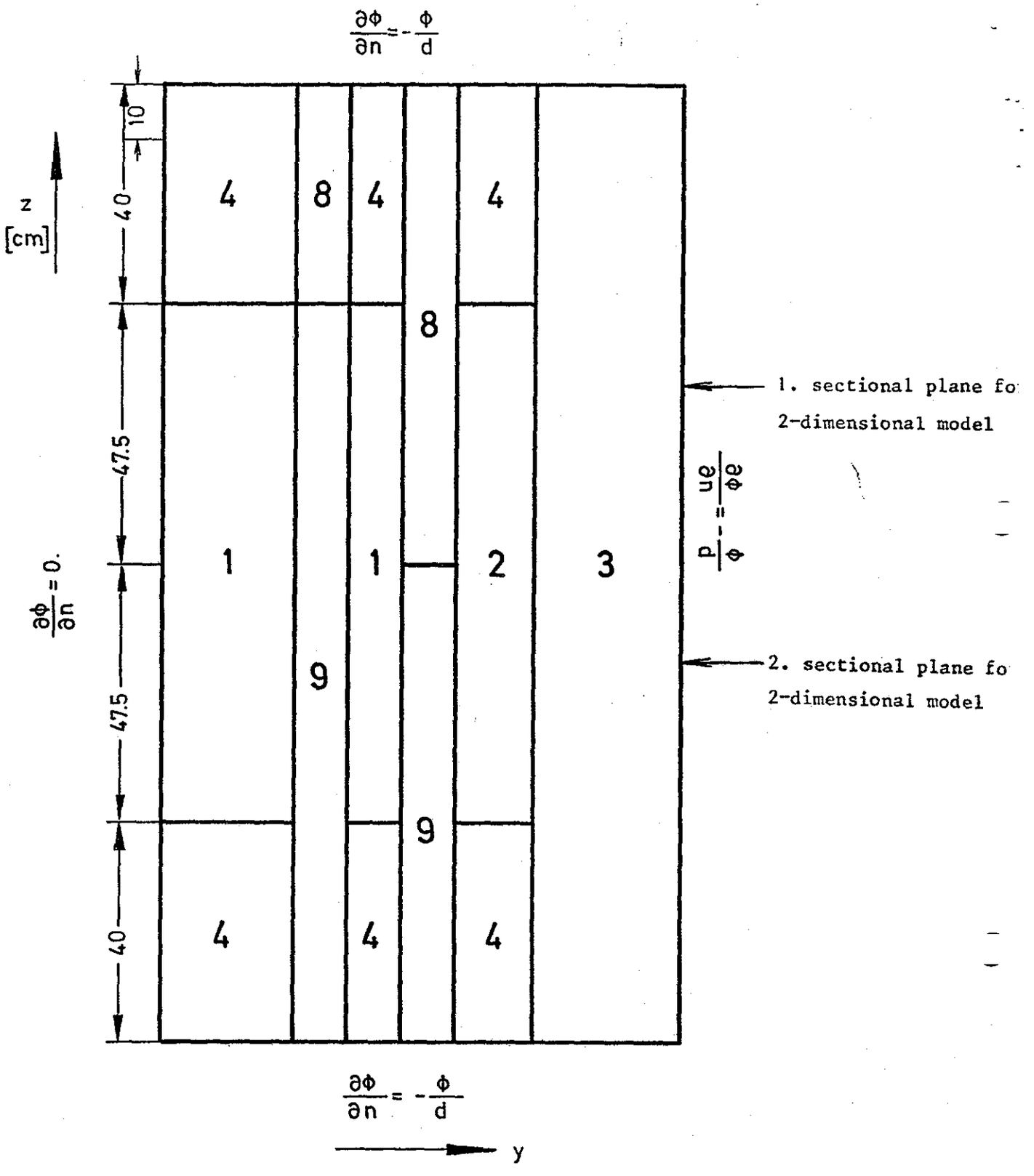

Fig. 2b): Transversal section of the benchmark problem in x y z geometry

86080010

Kernforschungszentrum Karlsruhe
Institut für Neutronenphysik
und Reaktortechnik

G.Buckel, R.Froehlich
K.Küfner, B.Stehle

January 2nd, 1975

(2-167)

A fast reactor benchmark problem in two and three space dimensions

There is a high need for benchmark problems in order to test and to compare the performance and accuracy of computational methods and of computer codes for the solution of reactor physics problems.

In what follows such a model-problem is described which has been designed mainly for neutron-diffusion calculations. The layout shown in pictures 1.a), 1.b), 2.a), 2.b) has its origin in the MARK I core design of the SNR 300, a sodium cooled fast breeder prototypereactor. Only some modifications have been made in oder to facilitate the representation of the reactor in the computer code input.

The whole benchmark problem consists of one three-dimensional model in triangular-z-geometry (see pict. 1.a), 1.b)) and a consistent one in rectangular x-y-z-geometry (see pict. 2.a), 2.b)). For each of the two geometries two twodimensional models have been developed. Relatively big homogeneous material zones have been chosen and the energy range is divided into four groups only, so input preparation and computing time should be reasonable. Note that the control-rods are inserted to different positions (see pict. 2.b)).

Table 1 gives the detailed composition of the different mixtures used (note that the mixture numbers 5, 6, 7 are neither defined there nor used in the layout), table 2 gives alternatively macroscopic cross-sections for all energy groups (which were obtained by a standard condensation process starting from the 26 group KFKINR cross section set).

86080011

The boundary conditions are chosen in such a way that pictures 1.a) and 1.b) resp. 2.a), and 2.b) represent one sixth resp. a quarter of the whole reactor. Outer boundary conditions are logarithmic, i.e. flux equal to zero at extrapolated boundaries . Note, that due to symmetries, as shown in picture 1.a), it is possible to calculate 30, 60, 90, 120, 180 and 360 degree sectors of the full reactor. The normal case however is considered to be the 120 degree sector.

For the twodimensional models the cutting planes (z= constant) are chosen such that (see pict. 1.b) and 2.b)) in the first model some control-rod positions contain absorber material and some follower material whereas for the second model only follower material is found in control-rod positions. For twodimensional calculations the buckling factor is assumed be zero.

For a realistic comparison of computing time it is proposed to start with a constant flux guess and to choose as "convergence criteria" for k_{eff} 10^{-4} (10^{-5}) and for fluxes 10^{-3} (10^{-4}). The values in parantheses are the values for twodimensional calculations. The detailed measuring of the convergence criteria should be explained in the documentation of the results.

86080012

TAB. 1: Atomic compositions (10^{+24} at/cm^3)

Comp. 1:	CR520	$0.334470 \cdot 10^{-2}$	Comp. 2:	CR520	$0.334470 \cdot 10^{-2}$
	FE560	$0.110890 \cdot 10^{-1}$		FE560	$0.110890 \cdot 10^{-1}$
	MO960	$0.156334 \cdot 10^{-3}$		MO960	$0.156334 \cdot 10^{-3}$
	NA230	$0.103501 \cdot 10^{-1}$		NA230	$0.103501 \cdot 10^{-1}$
	NB930	$0.104014 \cdot 10^{-3}$		NB930	$0.104014 \cdot 10^{-3}$
	NI590	$0.247123 \cdot 10^{-2}$		NI590	$0.247123 \cdot 10^{-2}$
	O 160	$0.124809 \cdot 10^{-1}$		O 160	$0.125310 \cdot 10^{-1}$
	PU400	$0.305554 \cdot 10^{-3}$		PU400	$0.443006 \cdot 10^{-3}$
	PU410	$0.347220 \cdot 10^{-4}$		PU410	$0.503416 \cdot 10^{-4}$
	PU420	$0.694441 \cdot 10^{-5}$		PU420	$0.100683 \cdot 10^{-4}$
	PU9A0	$0.104166 \cdot 10^{-2}$		PU9A0	$0.151025 \cdot 10^{-2}$
	U 5A0	$0.121290 \cdot 10^{-4}$		U 5A0	$0.106296 \cdot 10^{-4}$
	U 8A0	$0.483946 \cdot 10^{-2}$		U 8A0	$0.424120 \cdot 10^{-2}$
	V 510	$0.658087 \cdot 10^{-4}$		V 510	$0.658087 \cdot 10^{-4}$
Comp. 3:	CR520	$0.382146 \cdot 10^{-2}$	Comp. 4:	CR520	$0.336830 \cdot 10^{-2}$
	FE560	$0.123953 \cdot 10^{-1}$		FE560	$0.111654 \cdot 10^{-1}$
	MO960	$0.207136 \cdot 10^{-3}$		MO960	$0.157626 \cdot 10^{-3}$
	NA230	$0.699362 \cdot 10^{-2}$		NA230	$0.995783 \cdot 10^{-2}$
	NB930	$0.118841 \cdot 10^{-3}$		NB930	$0.104749 \cdot 10^{-3}$
	NI590	$0.310313 \cdot 10^{-2}$		NI590	$0.249052 \cdot 10^{-2}$
	O 160	$0.196203 \cdot 10^{-1}$		O 160	$0.138479 \cdot 10^{-1}$
	U 5A0	$0.245254 \cdot 10^{-4}$		U 5A0	$0.173099 \cdot 10^{-4}$
	U 8A0	$0.978563 \cdot 10^{-2}$		U 8A0	$0.690663 \cdot 10^{-2}$
				V 510	$0.657752 \cdot 10^{-4}$
Comp. 8:	B 100	$0.604851 \cdot 10^{-2}$	Comp. 9:	CR520	$0.260524 \cdot 10^{-2}$
	B 110	$0.247954 \cdot 10^{-1}$		FE560	$0.845038 \cdot 10^{-2}$
	C 120	$0.771097 \cdot 10^{-2}$		MO960	$0.141213 \cdot 10^{-3}$
	CR520	$0.410375 \cdot 10^{-2}$		NA230	$0.189532 \cdot 10^{-1}$
	FE560	$0.133110 \cdot 10^{-1}$		NB930	$0.810186 \cdot 10^{-4}$
	MO960	$0.222437 \cdot 10^{-3}$		NI590	$0.211552 \cdot 10^{-2}$
	NA230	$0.958653 \cdot 10^{-2}$			
	NB930	$0.127620 \cdot 10^{-3}$			
	NI590	$0.333236 \cdot 10^{-2}$			

86080013

TAB. 2: Macroscopic cross-sections for 4 energy groups

(Group constant set: KFKINR001)

Scheme of condensation in relation to 26 energy groups of ABN set:

group 1: 1,5 (10.5 - 0.8 MeV)
group 2: 6,11 (0.8 MeV- 10.0 KeV)
group 3: 12,14 (10.0 - 1.0 KeV)
group 4: 15,26 (1 KeV - therm)

Composition 1: Core, inner part
Composition 2: Core, outer part
Composition 3: radial blanket
Composition 4: axial blanket
Composition 8: absorber
Composition 9: follower

(The unusual numbering of compositions has been used because of extracting the compositions 1, 2, 3, 4, 8 and 9 out of a 17 composition cross section block)

CHI	group 1:	group 2:	group 3:	group 4:
M1	0.768	0.232	0.0	0.0
M2	0.768	0.232	0.0	0.0
M3	0.768	0.232	0.0	0.0
M4	0.768	0.232	0.0	0.0
M8	0.768	0.232	0.0	0.0
M9	0.768	0.232	0.0	0.0
NUSF				
M1	$0.11878 \cdot 10^{-1}$	$0.53252 \cdot 10^{-2}$	$0.10471 \cdot 10^{-1}$	$0.26611 \cdot 10^{-1}$
M2	$0.14943 \cdot 10^{-1}$	$0.76887 \cdot 10^{-2}$	$0.14809 \cdot 10^{-1}$	$0.38159 \cdot 10^{-1}$
M3	$0.77427 \cdot 10^{-2}$	$0.10825 \cdot 10^{-3}$	$0.29742 \cdot 10^{-3}$	$0.84687 \cdot 10^{-3}$
M4	$0.54279 \cdot 10^{-2}$	$0.75857 \cdot 10^{-4}$	$0.21218 \cdot 10^{-3}$	$0.57592 \cdot 10^{-3}$
M8	0.0	0.0	0.0	0.0
M9	0.0	0.0	0.0	0.0
SREM				
M1	$0.28204 \cdot 10^{-1}$	$0.52747 \cdot 10^{-2}$	$0.17612 \cdot 10^{-1}$	$0.26546 \cdot 10^{-1}$
M2	$0.28782 \cdot 10^{-1}$	$0.60491 \cdot 10^{-2}$	$0.19510 \cdot 10^{-1}$	$0.33714 \cdot 10^{-1}$
M3	$0.35959 \cdot 10^{-1}$	$0.58855 \cdot 10^{-2}$	$0.16041 \cdot 10^{-1}$	$0.13349 \cdot 10^{-1}$
M4	$0.29093 \cdot 10^{-1}$	$0.44909 \cdot 10^{-2}$	$0.13082 \cdot 10^{-1}$	$0.99562 \cdot 10^{-2}$
M8	$0.24814 \cdot 10^{-1}$	$0.16412 \cdot 10^{-1}$	$0.72122 \cdot 10^{-1}$	0.16868
M9	$0.13159 \cdot 10^{-1}$	$0.14559 \cdot 10^{-2}$	$0.46001 \cdot 10^{-2}$	$0.78660 \cdot 10^{-3}$

86080014

SFISS	group 1:	group 2:	group 3:	group 4:
M1	$0.39123 \cdot 10^{-2}$	$0.18286 \cdot 10^{-2}$	$0.36334 \cdot 10^{-2}$	$0.92415 \cdot 10^{-2}$
M2	$0.48531 \cdot 10^{-2}$	$0.26377 \cdot 10^{-2}$	$0.51332 \cdot 10^{-2}$	$0.13238 \cdot 10^{-1}$
M3	$0.27688 \cdot 10^{-2}$	$0.44347 \cdot 10^{-4}$	$0.12274 \cdot 10^{-3}$	$0.34952 \cdot 10^{-3}$
M4	$0.19453 \cdot 10^{-2}$	$0.31065 \cdot 10^{-4}$	$0.87566 \cdot 10^{-4}$	$0.23769 \cdot 10^{-3}$
M8	0.0	0.0	0.0	0.0
M9	0.0	0.0	0.0	0.0

STR				
M1	0.11587	0.21220	0.46137	0.34571
M2	0.11588	0.21213	0.46770	0.35349
M3	0.14584	0.28443	0.52703	0.40732
M4	0.12270	0.23133	0.46274	0.33749
M8	0.13317	0.25355	0.58044	0.54168
M9	$0.72206 \cdot 10^{-1}$	0.11487	0.32642	0.19272

SMTOT			
	1 → 2		
M1	$0.23597 \cdot 10^{-1}$		
M2	$0.23262 \cdot 10^{-1}$		
M3	$0.32071 \cdot 10^{-1}$		
M4	$0.26322 \cdot 10^{-1}$		
M8	$0.22946 \cdot 10^{-1}$		
M9	$0.12942 \cdot 10^{-1}$		
	1 → 3	2 → 3	
M1	$0.40791 \cdot 10^{-5}$	$0.16153 \cdot 10^{-2}$	
M2	$0.46451 \cdot 10^{-5}$	$0.15718 \cdot 10^{-2}$	
M3	$0.38880 \cdot 10^{-5}$	$0.27776 \cdot 10^{-2}$	
M4	$0.28907 \cdot 10^{-5}$	$0.22889 \cdot 10^{-2}$	
M8	$0.10320 \cdot 10^{-5}$	$0.37687 \cdot 10^{-2}$	
M9	$0.68780 \cdot 10^{-6}$	$0.12871 \cdot 10^{-2}$	
	1 → 4	2 → 4	3 → 4
M1	$0.44493 \cdot 10^{-7}$	$0.42309 \cdot 10^{-7}$	$0.46838 \cdot 10^{-2}$
M2	$0.49968 \cdot 10^{-7}$	$0.40724 \cdot 10^{-7}$	$0.43414 \cdot 10^{-2}$
M3	$0.45039 \cdot 10^{-7}$	$0.90018 \cdot 10^{-7}$	$0.58971 \cdot 10^{-2}$
M4	$0.33248 \cdot 10^{-7}$	$0.62133 \cdot 10^{-7}$	$0.53536 \cdot 10^{-2}$
M8	$0.10489 \cdot 10^{-7}$	$0.70361 \cdot 10^{-11}$	$0.86815 \cdot 10^{-2}$
M9	$0.69903 \cdot 10^{-8}$	$0.43633 \cdot 10^{-11}$	$0.34533 \cdot 10^{-2}$

86080015

SCAPT	group 1:	group 2:	group 3:	group 4:
M1	$0.73776 \cdot 10^{-3}$	$0.18315 \cdot 10^{-2}$	$0.93000 \cdot 10^{-2}$	$0.17323 \cdot 10^{-1}$
M2	$0.71134 \cdot 10^{-3}$	$0.18403 \cdot 10^{-2}$	$0.10041 \cdot 10^{-1}$	$0.20503 \cdot 10^{-1}$
M3	$0.11854 \cdot 10^{-2}$	$0.30639 \cdot 10^{-2}$	$0.10030 \cdot 10^{-1}$	$0.13012 \cdot 10^{-1}$
M4	$0.86927 \cdot 10^{-3}$	$0.21714 \cdot 10^{-2}$	$0.76478 \cdot 10^{-2}$	$0.97272 \cdot 10^{-2}$
M8	$0.18666 \cdot 10^{-2}$	$0.12645 \cdot 10^{-1}$	$0.63443 \cdot 10^{-1}$	0.16868
M9	$0.21684 \cdot 10^{-3}$	$0.16956 \cdot 10^{-3}$	$0.11497 \cdot 10^{-2}$	$0.78672 \cdot 10^{-3}$
1/V				
M1	$0.58026 \cdot 10^{-9}$	$0.24847 \cdot 10^{-8}$	$0.12547 \cdot 10^{-7}$	$0.31651 \cdot 10^{-7}$
M2	$0.58026 \cdot 10^{-9}$	$0.24847 \cdot 10^{-8}$	$0.12547 \cdot 10^{-7}$	$0.31651 \cdot 10^{-7}$
M3	$0.58026 \cdot 10^{-9}$	$0.24847 \cdot 10^{-8}$	$0.12547 \cdot 10^{-7}$	$0.31651 \cdot 10^{-7}$
M4	$0.58026 \cdot 10^{-9}$	$0.24847 \cdot 10^{-8}$	$0.12547 \cdot 10^{-7}$	$0.31651 \cdot 10^{-7}$
M8	$0.58026 \cdot 10^{-9}$	$0.24847 \cdot 10^{-8}$	$0.12547 \cdot 10^{-7}$	$0.31651 \cdot 10^{-7}$
M9	$0.58026 \cdot 10^{-9}$	$0.24847 \cdot 10^{-8}$	$0.12547 \cdot 10^{-7}$	$0.31651 \cdot 10^{-7}$

86080016

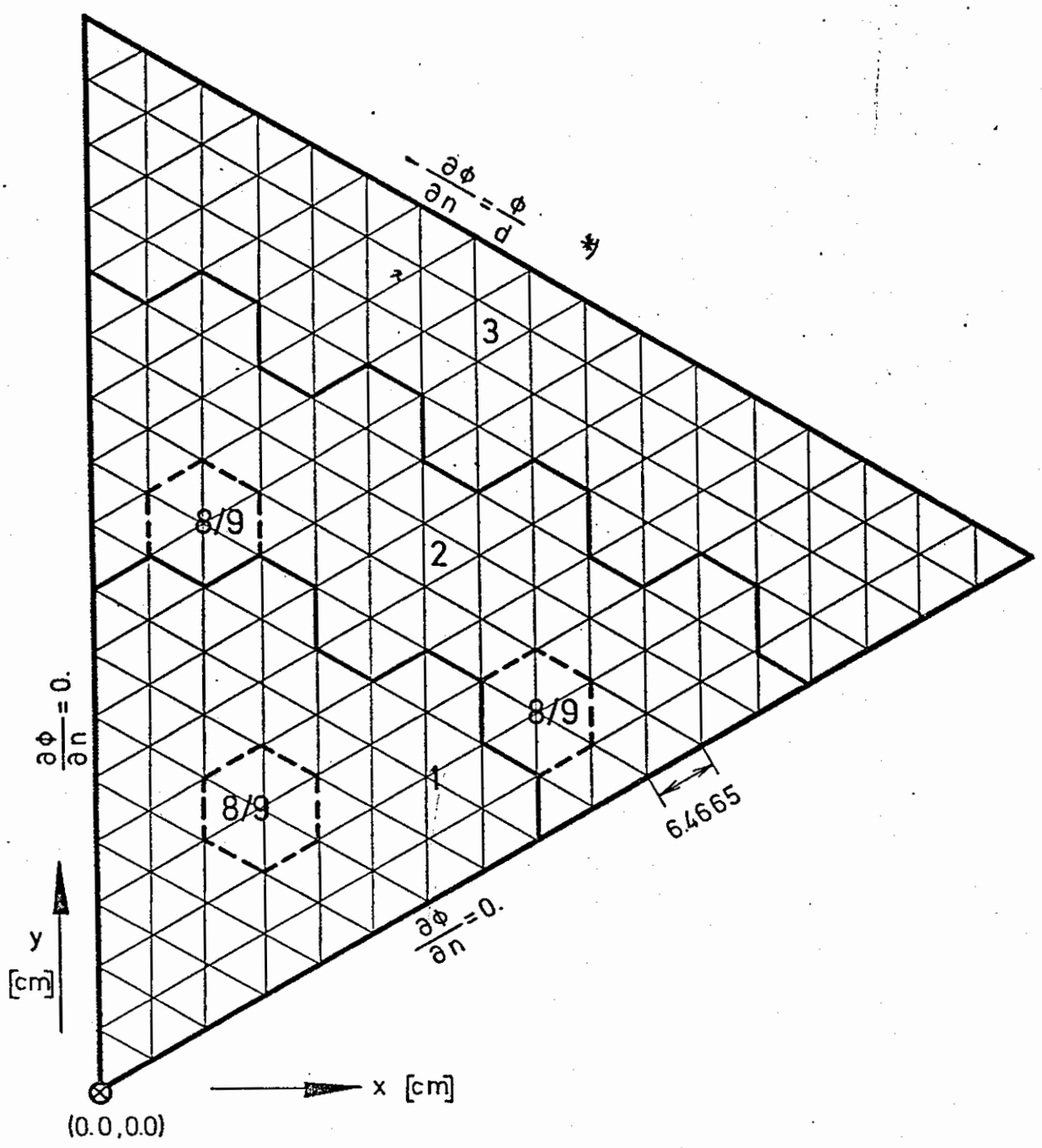

*) $d = 0.71 \cdot \lambda_{tr}$

1: Core, inner part
2: Core, outer part
3: radial blanket
4: axial blanket
8: absorber rod
9: follower

Fig. 1a): Axial section of the benchmark problem for triangular geometry

86080017

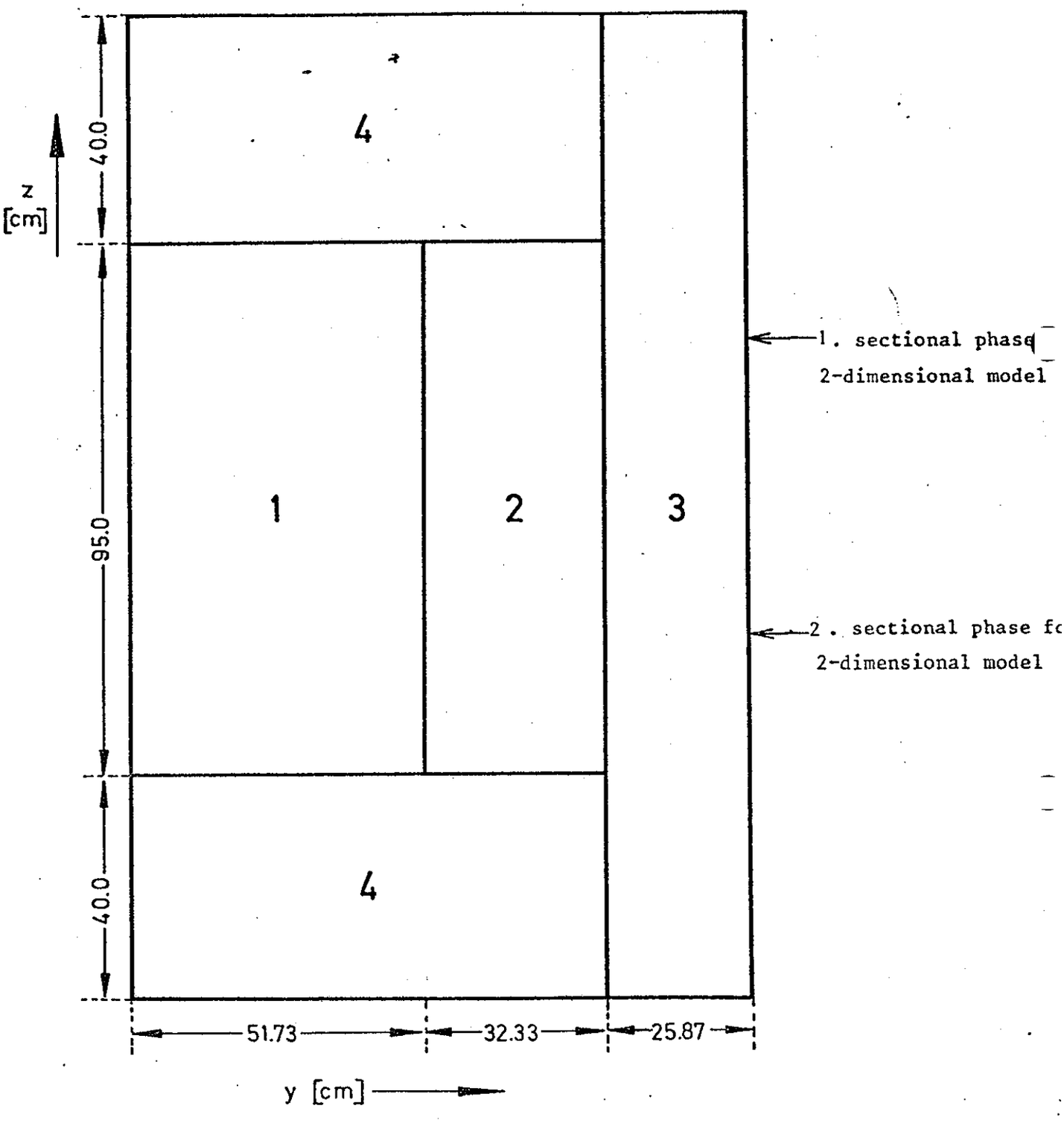

Fig. 1b): Transversal section of the benchmark problem for triangular geometry (x = y = 0.)

86080018

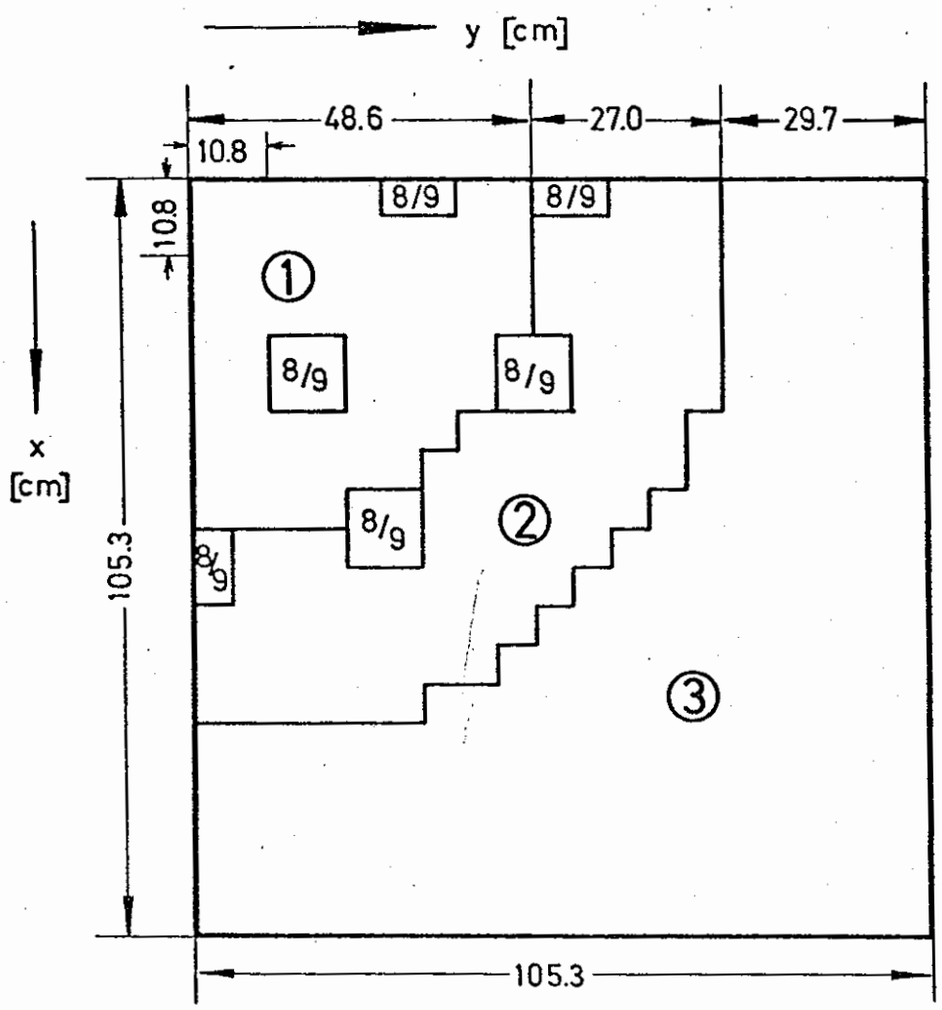

Boundary conditions:

Left and upper boundary: $\frac{\partial \Phi}{\partial n} = 0.$

otherwise: $\frac{\partial \Phi}{\partial n} = -\frac{\Phi}{d}$

Fig. 2a): Axial section of the benchmark problem in x y z geometry

86080019

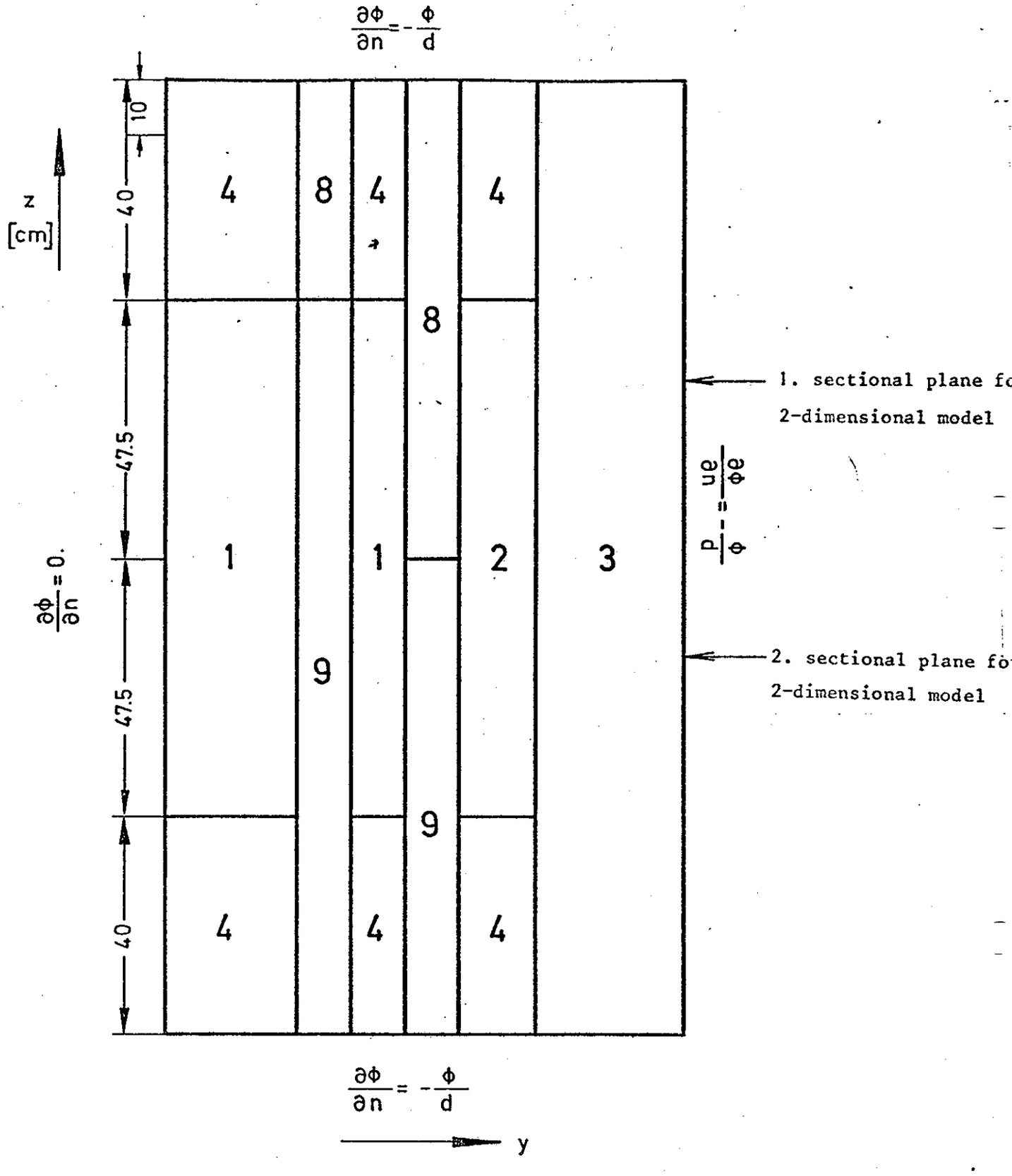

$d = 0.71 \cdot \lambda_{tr}$

Fig. 2b): Transversal section of the benchmark problem in x y z geometry

86080020

February, 1976

L-175

Results and Main Conclusions of the IAEA-Advisory Group Meeting on Transactinium Nuclear Data, held at Karlsruhe, November 1975

by

H. Küsters and M. Lalović

1. Objectives of the Meeting

The meeting was held November 3-7, 1975 at the Nuclear Research Center Karlsruhe. About 50 scientists from research and industrial institutions of 16 countries had followed the invitation by IAEA to discuss the following objectives:

a) Review of the present situation regarding the use of TND in reactor and non-reactor applications, specification of nuclear data requirements and their priorities.

b) Review of the status of knowledge of TND, including a critical comparison of existing evaluations and compilations.

c) Identification and discussion of TND measurements, compilations and evaluations required to satisfy user needs.

With a view to these objectives the meeting was organized into three main sessions:

A. Review of TND applications by the users (reactor and non-reactor applications).

B. Review of TND Status.

C. Detailed discussion of A and B and specification of recommendations.

86080021

2. Application and Requirements of TND (Session A)

The importance of TND in reactor applications comes from the following problems (in this contribution we exclude the dominating isotopes as U235, U238, Pu239):

a) Reactor Operation including Recycling of Fuel

The main interest with respect to TND isotopes is their influence on the reactivity of the system via absorption and (spontaneous and induced) fission processes.

b) Reactor Shutdown

1. The shutdown reactivity margin has to be within the requested bounds, which are influenced by spontaneous fission of heavy actinides (sub-criticality).
2. The produced heat after shutdown, mainly by β^- and γ-emission of heavy nuclei, determines the energency core cooling layout.

c) Transport, Reprocessing and Refabrication of Spent Fuel

The prediction of radiation and heat level depends on the neutron, γ-, α^- and β-output of spent fuel and has to be known for the design of appropriate shielding and cooling devices.

d) Fuel Waste

Non-recovered fuel forms a potential hazard because of its contents of long-lived α-emitting isotopes of the heavy elements Np, Pu, Am and Cm (besides fission products). Therefore the in-pile production rate of these isotopes and the out-of-pile decay rate is of prime interest.

As a guideline the main isotopes contributing to the various items above are listed in Table 1 for reactor systems of present interest. (The results are based on ORIGEN (version 1973) calculations).

86080022

BY DISCHARGE	L W R (1000 MWe)	L M F B R (2000 MWe)	H T G R (1000 MWe)
CONCENTRATION [gr / Ton Heavy M.]	U238 $9.6\cdot10^5$ U235 $9.2\cdot10^3$ Pu239 $8\cdot10^3$ U236 $6.7\cdot10^3$ Pu240 $2.4\cdot10^3$ Pu241 $1.7\cdot10^3$ Np237 $9.4\cdot10^2$ Pu242 520. Pu238 475. Am243 209 Cm244 108. Am241 42. Cm242 21.	U238 $1.5\cdot10^6$ Pu239 $1.9\cdot10^5$ Pu240 $7.9\cdot10^4$ Pu241 $2.9\cdot10^4$ Pu242 $1.4\cdot10^4$ Am241 $3.\cdot10^3$ Am243 $5.7\cdot10^2$ Np237 300. U236 250. Pu238 94. Cm242 62. Am242M 31. Cm244 19.	Th232 $8.6\cdot10^5$ U233 $2\cdot10^4$ U234 $1.5\cdot10^4$ U235 $1\cdot10^4$ U238 $3\cdot10^3$ Np237 $2\cdot10^3$ Pu238 $1\cdot10^3$ Pu239 $2.7\cdot10^2$ Pu241 97. Pu240 92. Cm244 5. Am241 4.
THERM. POWER [Watt / Ton Heavy M.]	Np239 $3.1\cdot10^4$ Cm242 $2.6\cdot10^3$ U237 $1\cdot10^3$ Pu238 $2.7\cdot10^2$	Np239 $8.8\cdot10^4$ Cm242 $7.6\cdot10^3$ Pu240 543. Am242 472. Pu239 370 Am241 347	Pa233 $3.9\cdot10^4$ Pa234M $2\cdot10^3$ Np239 $6.4\cdot10^2$ Pu238 $6\cdot10^2$
Sp. Fiss. [NEUTR/SEC]	Cm244 $1.2\cdot10^9$ Cm242 $4.2\cdot10^8$ Cm246 $1.3\cdot10^7$ Pu240 $2.2\cdot10^6$ Pu238 $1.1\cdot10^6$	Cm242 $1.2\cdot10^9$ Cm244 $2.2\cdot10^8$ Pu240 $7.4\cdot10^7$ Pu242 $2.8\cdot10^7$ Pu238 $2.2\cdot10^5$	Cm244 $6.3\cdot10^7$ Cm242 $1.5\cdot10^7$ Pu238 $2.5\cdot10^6$ Cm246 $5.5\cdot10^5$
(α,n) [NEUTR/SEC]	Cm242 $2\cdot10^8$ Cm244 $2\cdot10^7$ Pu238 $1.6\cdot10^7$ Pu240 $8.4\cdot10^5$	Cm242 $6.\cdot10^8$ Pu240 $2.8\cdot10^7$ Am241 $2.1\cdot10^7$ Pu239 $1.9\cdot10^7$ Cm244 $3.8\cdot10^6$	Pu238 $3.6\cdot10^7$ Cm242 $7.7\cdot10^6$ Cm244 $1\cdot10^6$ U232 $3.7\cdot10^5$
HAZARD. INDEX [m^3]	Np239 $2.3\cdot10^{11}$ U237 $1.6\ 10^{10}$ Cm242 $3.5\cdot10^9$ Pu238 $1.6\cdot10^9$ Cm244 $1.2\cdot10^9$ Am242 $1.2\cdot10^9$ Pu241 $9\cdot10^8$	Np239 $6.5\cdot10^{11}$ Pu241 $1.5\cdot10^{10}$ Cm242 $1.\cdot10^{10}$ U237 $3.6\cdot10^9$ Pu240 $3.5\cdot10^9$ Am242 $3.5\cdot10^9$ Am241 $2.6\cdot10^9$ Pu239 $2.4\cdot10^9$	Pa233 $2.9\cdot10^{11}$ Np239 $4.7\cdot10^9$ Pu238 $3.7\cdot10^9$ Cm242 $1.3\cdot10^8$ Th234 $9.3\cdot10^7$ Cm244 $6.4\cdot10^7$

Tab. 1 Contribution of various Actinides in Composition and Radiation Output at Discharge of Reactor Fuel.

860800023

For 1000 years after discharge of fuel, the relative contribution of the main isotopes to the waste hazard index is as follows:

1. PWR: (Am241 : Am243 : Pu240 : Pu239 : Cm245) ≈ (16 : 9 : 5 : 1 : 0,5)
2. LMFBR: (Am241 : Pu240 : Am243 : Pu239 : Pu238) ≈ (70 : 3 : 3 : 3 : 0,1)

According to the various papers presented, the most restrictive requirements for TND in reactor applications at present are given by the effect these nuclei have on core performance. For the cross sections of the heavy nuclei such as $U23^3$, U235, U238, Pu239, Pu240, Pu241 and Pu242, data requests are already formulated in WRENDA; accuracies of about 5 % or better are requested.

According to Barré and Bouchard (paper A2), the reactivity effects of the various nuclides were calculated and are listed in Table 2 (the main actinides such as U235, U238 and Pu239 are not included).

Tab.2: Reactivity Effects of Actinides in Thermal and Fast Reactors.

Reactivity	Thermal Reactor 30000 $\frac{MWd}{t}$ PWR		Fast Reactor (1300 MWe)	
$\frac{\delta k}{k}$	Uranium Fuel	Pu-Recycling	Burnup 0	Burnup 120.000 MWd/t
$> 10^{-2}$	U236,Pu240,Pu241	U236,Pu240,Pu241	Pu240,Pu241,Pu242	Pu240,Pu241,Pu2
10^{-3} to 10^{-2}	U234,Np237,Pu242	U234,Np237,Pu241 Am241,Am243	Pu238,Am241	Pu238,Am241, Am242,Am243
10^{-4} to 10^{-3}	Pu238,Am241, Am243,Am242m	Pu238,Am242m		Am242,Cm244,Np2 Np239
10^{-5} to 10^{-4}		Cm242,Cm243,Cm244	Np237	Cm243

8608002

For a thermal HTR the main influence on the reactivity, apart from Th and U233, is given by Pa231, U232, U234.

The effect on other core parameters such as power and breeding gain is again dominated by the higher Pu-isotopes; in a fast reactor the contribution to reactor power by Pu240/Pu241/Pu242 is about 6%/8%/1%, whereas in thermal reactors only Pu241 is of importance (2-3% for uranium fuelled cores, 5 to 10 % for Pu-recycled systems). The other actinides contribute in a fast system less than 1 % each, in total about 1 %. Pu240 is essential for its influence on the thermal neutron spectrum, but no major deficiencies have shown up to date. At the end of fuel life Am241 may have an effect on the breeding gain by about 0.02.

According to these investigations the cross section data most urgently needed are those for the higher Pu isotopes (including Pu238) and Am241, Am242m and Am243; in particular those for fast reactors, as the main data gaps exist in the epithermal and fast energy region. This is being stressed by experimental results from fast zero-power reactors, where e.g. the prediction of the capture-to-fission ratio for Am241 deviates by a factor of about 2 from experimental results (paper A3). In thermal systems the data are known to better accuracy.

It should be kept in mind that generally the formation of the α-emitters Am and Cm does depend more strongly on the cumulated cross section uncertainties of the preceding isotopes in the corresponding chains than on the cross sections of the "reference nuclide" itself. For instance, Cm244 with 18y half-life is formed via 3 routes: via $Pu241 \xrightarrow{\beta} Am241 \xrightarrow{n\gamma} Am242 \xrightarrow{\beta} Cm242 \xrightarrow{n\gamma} Cm243$ and via $Pu241 \xrightarrow{n\gamma} Pu242 \xrightarrow{n\gamma} Pu243 \xrightarrow{\beta} Am243 \xrightarrow{n\gamma} Am244$, the latter being by far the dominant route because of the competing strong α-emission of Cm242. A third route is given by $Pu241 \xrightarrow{\beta} Am241 \xrightarrow{n\gamma} Am242m \xrightarrow{n\gamma} Am243 \xrightarrow{n\gamma} Am244 \xrightarrow{\beta} Cm244$. Thus the uncertainty in Cm244 content is given by the uncertainties in Pu242, Am242m and Am243 capture data and by the absorption rate uncertainty for Cm244.

Data for the first three isotopes are estimated to have an uncertainty of about 20 % and 50 %, respectively, and the estimate for Cm244 is about 50 %. If cross section uncertainties tend to be on one side of the true value systematic error, then the uncertainty in the Cm244 cross section partially compensates the cumulated uncertainty of the formation process.

86080025

The out-of-pile behaviour of actinides is mainly determined by two facts: (1) the actinide concentration at discharge from the reactor and (2) their corresponding decay properties. With regard to neutron production in addition to spontaneous fission the occurence of (α,n) processes, especially with oxygen, is to be considered, but the neutron production is about an order of magnitude less than that from spontaneous fission. From this fact it follows that cross sections play a minor rôle after discharge of burnt fuel. Therefore, the main objective in discussing the sensitivity of the radiation output from spent fuel to cross section changes is in establishing the corresponding variation in nuclide concentration at discharge from the reactor.

First of all, it is of primary interest to compare calculated and measured nuclide concentrations for various power reactor systems. Some of the available material is discussed by Küsters and Lalović (paper A3). Apart from the uncertainty in calculational methods, which, in principle, can be relatively small if sophisticated tools are used, the major uncertainty in the theoretical prediction of nuclide concentrations arises from reactor operation changes and often not fully known irradiation and flux histories of the discharged elements. Therefore the calculated U238 content in spent fuel is sometimes adjusted to the experimental value. For PWR fuel, however, this approach causes changes of up to about 40 % in the concentrations of less dominating actinide isotopes, e.g. in the Cm244 content. With simplified models (e.g. fundmental-mode calculations) the differences are even larger and must be expressed sometimes by factors.

A sensitivity analysis shows (A3) that for various times after discharge the radiation hazard is uncertain by about 20 to 50 %, if plausible uncertainties in nuclear data are assumed.

Quite generally, the dominating cause for differences in nuclide concentration and radiation output is given by the composition, the fuel cycle strategy (e.g. Pu recycling or uranium fuel cycle for PWRs) and the degree of burn-up of the reactor fuel; these effects may amount to about a factor of 10 e.g. in hazard potential for a PWR with and without Pu recycling. In addition, one has to keep in mind that for about 500 years after discharge the fission products cause most of the radiologic hazard. After that the actinides dominate

86080026

mainly with α-emission from Am, until after several thousand years the long-lived Pu isotopes give the main contribution to radioactivity from a unit of discharged reactor fuel.

With regard to the decay properties of nuclei, quite generally uncertainties in decay constants λ cause uncertainties of the same order of magnitude in the concentration e.g. of α-emitters at a decay time equal to the half-life. This is only approximately true because due to the decay of other nuclides the reference nuclide may increase in concentration. In other words, without this feedback and without external manipulation, a 10 % change in λ results in a 10 % change of nuclide concentration at $t = 1/\lambda$.

At present uncertainties in decay constants are about 10 % or smaller, thus the related effects are not very important.

Transmutation of actinides in reactors was being considered at the meeting by Koch (paper A6) as an alternative to waste storage. In this case there is a definite need for cross sections (fission and capture) of the long lived α-emitters. From a physical point of view reactors with hard neutron spectra (σ_c/σ_f small) are to be preferred. At present nuclear industry is not particularly interested in this topic; the waste storage strategy (e.g. in salt mines) is the favoured route for waste disposal. In this connection there was a discussion of separation of the α-emitters Am, Cm and others from spent fuel. The necessary separation technology, however, is not likely to become available within the next two decades.

Very restrictive requirements (0.5 to 1 %) for the half-lives of the Pu-isotopes were stated by Dierckx (paper A8) in order to obtain sufficiently accurate results for the analysis of non-destructive and destructive techniques to determine the isotopic contents of spent fuel; these measurements are made for small waste residues and for safeguard purposes. It is not quite obvious, whether safeguard techniques, which are usually based on realtive measurements, do require such high precision.

The situation is different in the field of non-reactor applications of TND. Aten (paper A9) points out that e.g. for application in health physics and for purity tests high accuracies are required for α-, β-, γ- and X-ray energies, not to mention the question of standards.

86080027

3. Status of TND (Session B)

The difficulties of experimental techniques for the measurement of TND will be summarized briefly. Also the present situation regarding availability of evaluated TND on nuclear data files will be given as well as the capability of nuclear theory.

3.1 Differential measurements on TND

The main objective is the determination of fission and capture cross sections. A major difficulty in cross section measurements of the actinides is in obtaining pure isotopic samples; either they are not readily available or they are available only in very small quantities. Thus data for many of the higher actinides are fragmentary or non-existent. Sample preparation costs for most of the higher actinides are rather high; impurities and the activity of the samples require very sophisticated techniques to obtain reliable cross section data.

According to James (paper B2) some improvements in experimental techniques have been acchieved recently. In the resonance region resonance spins were measured by using polarized neutron beams and polarized targets; low-energy resonances having meV fission widths in the U238 subthreshold fission cross section could be detected at RPI with a Linac-pulsed neutron source in a lead slowing-down spectrometer. The Saclay group used successfully a large gas scintillator chamber cooled to liquid-nitrogen temperature for the measurement of fission cross sections. A spherical design of an ionization chamber by Dabbs reduces the maximum possible alpha path length and thus α pile-up. At ORELA fission cross section measurements could be performed on an isotope with only 30y α half-life. Spark chambers have the great advantage of spatial resolution in countering α pile-up but suffer from spontaneous sparking background. If oxides and light elements are used for encapsulation, fission neutron detectors with pulse shape discrimination do overcome the α pile-up, but then background from (α,n) processes is produced.

For highly radioactive actinide isotopes with half-lives of days of longer the nuclear explosion technique has been used for neutron cross section measurements by time of flight at Los Alamos (paper B3). The accuracy of the data is not high, one has to except a typical total uncertainty for fission and capture cross sections of about 10 - 30 % over the intermediate and fast neutron energy

86080028

region. Data (mainly fission cross sections) for the following nuclides have been obtained and are available from the four neutron data centers: Th230, Pa231, U232, U234, U236, U237, Np237, Pu239, Pu240, Pu241, Pu242, Pu244, Am241, Am242m, Am243, Cm243, Cm244, Cm245, Cm246, Cm248, Cf249, Cf252, Es253.

To give an impression on the availability of differential measurements, in Table 3 the present gaps in experimental data for the various nuclei and the corresponding energy regions are given (see paper A1).

3.2 Evaluation of TND and Capability of Nuclear Theory

Because there are many gaps in differential nuclear data for actinides, the evaluation must rely heavily on nuclear reaction theory. In the thermal range the cross sections are calculated from resonance parameters by means of resonance theory. In the resolved-resonance range the Breit-Wigner single level formula is used most frequently, but for the fission cross sections also multilevel representations. The Lane-Lynn formalism is adopted for the calculation of average cross sections in the unresolved range. Optical-model and statistical theories are applied in the fast neutron energy range. On the basis of both differential data (if available) and nuclear theory, nuclear data for actinides have been evaluated in the last years (see paper B5a).

Table 4 gives a summary of the present status (Notation in Tab.4:
E4 ≡ ENDFB/IV; K ≡ KEDAK; LLL ≡ Lawrence Laboratory Livermore.

References of Tab. 4 can be found in Appendix 1.

It is interesting to note Lynn's remarks (paper B5b) on the degree of confidence which can be placed on the results of present model calculations. He estimates the uncertainty of cross sections of a statistical of integral character (e.g. capture, fission, summed inelastic scattering, etc.) for transactinium nuclei to about 25 - 30 % (U, Np, Pu, Am, Cm244, Cm245), being rather worse for the very high transplutonium elements (± 50 %) and for cross sections of more specific character (e.g. radiative capture populating an isomeric state as in Am242m.) While these uncertainties are poorer than the degree of accuracy attainable with very careful experimental techniques, this accuracy

860800029

TAB.3: GAPS in $\sigma(E)$ for Energy Intervals (ΔE in MeV)

ELEMENT	TYPE of Cross Section						
		Th227	Th228	Th231	Th232	Th234 Th233	
Th	t	0.-15.	0-$2\cdot10^{-6}$ $1\cdot10^{-5}$-15	0-15	-	0-15	
	n,γ	0.-15.	0-15	0-15	$2\cdot10^{-8}$-$1\cdot10^{-7}$ $3\cdot10^{-6}$-2	0-15	
	n,f	$2\cdot10^{-8}$-15	0-0.2 1-15	0-15	0-0.7	0-15	
		Pa230	Pa231	Pa232	Pa233		
Pa	t	0-15	0.002-15	0-15	0.01-15		
	n,γ	0-15	E_{th}-0.1 6-15	E_{th}-15	E_{th}-15		
	n,f	0-15	E_{th}-0.1 4-15	E_{th}-15	E_{th}-15		
		U231	U232	U234	U236	U237	U238	U239
U	t	0-15	0.01-15	0.001-15	0.001-15	0-15	E_{th}-$1\cdot10^{-6}$	0-15
	n,γ	0-15	E_{th}-15	E_{th}-15	$1\cdot10^{-6}$-0.06	E_{th}-15	E_{th}-$7\cdot10^{-6}$	E_{th}-15
	n,f	E_{th}-15	E_{th}-$7\cdot10^{-6}$ 0.02-0.15 1.5-15	E_{th}-$2\cdot10^{-2}$ 0.02-0.15 6-15	E_{th}-$8\cdot10^{-5}$ 6-15	E_{th}-$7\cdot10^{-5}$ 2-15	-	E_{th}-15
		Np236	Np237	Np238	Np239			
Np	t	0-15	0.01-15	0-15	0-15			
	n,γ	0-15	E_{th}-0.15	0-15	E_{th}-15			
	n,f	E_{th}-15	E_{th}-$1\cdot10^{-7}$	E_{th}-15	E_{th}-15			
		Pu238	Pu240	Pu241	Pu242			
Pu	t	0.01-15	0.007-0.1 1.5-15	0.001-15	0.009-15			
	n,γ	E_{th}-$1\cdot10^{-5}$ 0.2-15	0.5-15	0.1-15	E_{th}-15			
	n,f	-	E_{th}-$5\cdot10^{-7}$	-	E_{th}-$7\cdot10^{-5}$			
		Am241	Am242	Am242m	Am243	Am244		
Am	t	$6\cdot10^{-5}$-15	0-15	0-15	0.001-15	0-15		
	n,γ	0.4-15	0-15	0-15	E_{th}-15:	0-15		
	n,f	8-15	E_{th}-$2\cdot10^{-5}$ 1-15	0-15	E_{th}-$7\cdot10^{-5}$ 4-15	E_{th}-15		
		Cm242	Cm243	Cm244	Cm245	Cm246		
Cm	t	0-15	0-15	E_{th}-$7\cdot10^{-6}$ $7\cdot10^{-4}$-15	E_{th}-15	$6\cdot10^{-5}$-15.		
	n,γ	E_{th}-15	0-15	E_{th}-$2\cdot10^{-5}$ 0.01-15	E_{th}-15	E_{th}-15.		
	n,f	0-15		E_{th}-$2\cdot10^{-5}$ 4-15	E_{th}-$2\cdot10^{-5}$ 4-15	E_{th}-$2\cdot10^{-5}$ 4-15		

86080030

ISOTOPES	File and/or Reference	Latest Data Revision	Energy Range [eV]
Pa231, Pa233, U232	Drake 67(1)	1967	10^{-3}-$15 \cdot 10^{6}$
P233	E4, Young 70 (unpub.)	1974	10^{-5}-$20 \cdot 10^{6}$
U234	E4, Drake 67A(2)	1967	10^{-5}-$20 \cdot 10^{6}$
U236	E4, Drake 67A(2) McCrosson 71 (unpub.)	1971	10^{-5}-$20 \cdot 10^{6}$
U236	Parker 64(3)	1964	10^{3}-$15 \cdot 10^{6}$
U237	Caner 75 (to be pub.)	1975	10^{4}-$7 \cdot 10^{5}$
Pu238, Pu242, Cm244	E4, Dunford 67(4)	1967	10^{-5}-$20 \cdot 10^{6}$ (E4)
Pu238	Caner 74 (6)	1974	10^{-3}-$15 \cdot 10^{6}$
U232, U236, Pu238, Pu240	Thomet 74 (8,7)	1974	$3 \cdot 10^{3}$-10^{6}
Pu240	E4, Pennigton 74 (unpub.) Hunter 73(9)	1974	10^{-5}-$20 \cdot 10^{6}$
Pu240	K, Caner 73 (11, 12)	1973	10^{-3}-$15 \cdot 10^{6}$
Pu241,Pu242	K, Caner 73A (12, 13, 14)	1973	10^{-5}-$20 \cdot 10^{6}$
Np237	E4, Smith 69(15)	1973	10^{-5}-$20 \cdot 10^{6}$
Pa231, U232, U234, U236, U237, Np237, Np238, Pu236, Pu238, Am241, Cm242	Hinkelmann 70(16)	1970	0.025 - $10 \cdot 10^{6}$
Pu241	E4, Hummel 73 (unpub.)	1974	10^{-5}-$20 \cdot 10^{6}$
U238, Pu239, Pu240, Pu241	Prince 70 (5)		10^{4}-$15 \cdot 10^{6}$
U236, Np237, Pu238, Pu240, Pu241, Pu242, Am241, Am243, Cm244	Pearlstein 66 (10)	1966	0.025 - $2 \cdot 10^{2}$
Am241, Am243	E4, Smith 66 (unpub.)	1966	10^{-5}-$20 \cdot 10^{6}$
Cm245, C_f252	LLL, Howerton 75 (unpub.)	1974	thermal - $20 \cdot 10^{6}$
C_f252	Prince 69 (17)	1969	0.025 - $15 \cdot 10^{6}$

Tab.4: Survey of Recent Evaluations on TND.

86080031

might be reasonable for those isotopes for which differential measurements have not been performed. To obtain a better prediction of cross section data, Lynn demands improvements in models and parametrisation: For total cross section elastic scattering, compound nucleus formation and neutron transmission coefficients the coupled-channel version of the optical model needs to be explored; level density formulations in particular provide a great area of uncertainty; considerable ignorance exists on the detailed mechanisms of radiative capture and also of neutron induced fission.

4. Requirements for TND

According to the discussion and recommendations of 3 subgroups, the required accuracies for TND were specified. The requests should be considered as estimates, which reflect personal judgement and are only rarely based on thorough sensitivity analyses. As outlined in section 2 of this summary, the main reason may be that the effects of TND are swamped by the effects of fission products (for the first few hundred hears after fuel discharge) and by the differences in e.g. material composition, burn-up and fuel cycle strategy in power reactors of present interest.

In Table 5 we have listed the various requests for TND. (Remark: If no request was formulated, the corresponding position in the table as well as the status were left empty.)

Recommendations for further measurements on TND may be deduced from Tab. 5, and can be found in more detail in the redommendations of the subgroup discussions, which will be included in the proceedings of the meeting. Priority in measurement and evaluation should be put on data of the higher plutonium and americium isotopes. For americium, especially neutron radiative capture data and branching ratios are unknown or very uncertain.

86080032

Isotope	Half-Life $T_{1/2}$	Decay Properties: Type	Decay Properties: Accuracy (%) Requested	Decay Properties: Accuracy (%) Status	Cross Sections: Type Therm. React.	Cross Sections: Type Fast React.	Cross Sections: Accuracy (%) Request Therm.	Cross Sections: Accuracy (%) Request Fast	Cross Sections: Accuracy (%) Status Therm.	Cross Sections: Accuracy (%) Status Fast
Pa231	$1 \cdot 10^4$Y				C/I_c		10/20		10/7	
Pa233	27.d				C/I_c		10/10		12/4	
Th232	$1 \cdot 10^{10}$Y				(n,2n)		50		-	
U232	74Y				$C/I_c/F/I_f$		30/30/30/30		2/6/12/15	
U233	$1.6 \cdot 10^5$Y				(n,2n)		10		-	
U234	$2.5 \cdot 10^5$Y	α-Intensity	1	3	C/I_c		5/5		2/12	
U236	$2.4 \cdot 10^7$Y	λ	1	2	C/I_c		4/4		6/6	
U237	6.7d				C/I_c		100/100		33/18	
Np237	$2.2 \cdot 10^6$Y	α-Intensity	1	20	C/I_c	C,F,(n,2n)	100/10	30/50/50	2/8	50/10/-
Np239	2.3d				C	C/F	100	20/50		/-
Pu236	2.8Y				C/I_c	C/F	100/100	50/50	-/-	-/-
Pu238	86.4Y	λ/ (γ/α)-Int.	0.5/1/0.1	1.5/25/1	$C/I_c/F$	C/F	30/50/50	20/7	4/10/3	30/10
Pu240	$6.6 \cdot 10^3$Y	λ/ (γ/α)-Int.	0.2/1/0.2	$5/^{Fact}_4/1$	C/I_c		2/1	*	1/12	
Pu241	13.2Y	λ/γ-Int.	1/1	5/5	$C/I_c/F$		3/10/1	*	3/5/1	
Pu242	$3.8 \cdot 10^5$Y	λ/α-Int.	1/4	5/10	C/I_c		10/5	*	4/4	
Am241	458Y	γ-Intensity	1	2	C/I_c	C/F	10/10	5/15	3/9	30/30?
Am242M	152Y				$C/I_c/F$	C/F	50/50/30	50/15	-/-/4	-/50
Am243	795Y				C/I_c	C/F/(n,2n)	15/10	10/30/50	5/3	-/10/-
Cm242	163d	λ	0.1	1	C/I_c	C/F	50/50	50/25	50/30	-/-
Cm243	35Y				$C/I_c/F$	C/F	50/50/50	30/20	-/-/7	-/-
Cm244	18Y				C/I_c	C/F	50/50	50/50	20/10	-/30?

* Requests according to WRENDA

Tab.5: Comparison of Requested and Achieved Accuracy of TND.

Notation:

C: Capture — I_c: Resonance Integral for neutron capture

F: Fission — I_f: Resonance Integral for neutron fission

86080033

Appendix 1

References for Table 4

1 DRAKE, M.K., NICHOLS, P.F., Ga-7462 (1967)

2 DRAKE, M.K., NICHOLS, P.F., GA-8135 (1967)

3 PARKER, K., AWREO-30/64 (1964)

4 DUNFORD, C.L., ALTER, H., NAA-SR-12271 (1967)

5 PRINCE, A., Proc. 2nd. Int. Conf. Nucl. Data for Reactors, IAEA (1970) Vol. II, 825.

6 CANER, M., YIFTAH, S., IA-1301 (1974); also: Nucl. Sci. Eng. (to be published).

7 THOMET, P., CEA-R-4631 (1974)

8 THOMET, P., JAERI - M 5984 (1975) 71.

9 HUNTER, R.E., STEWART, L., HIRONS, T.J., LA-5172 (1973)

10 PEARLSTEIN, S., BNL 982 (1966)

11 CANER, M., YIFTAH, S., IA-1243 (1972)

12 CANER, M., YIFTAH, S., SHATZ, B., MEYER, R., Proc. Int. Symp. Fast Reactor Phys., Tokyo (1973) 683.

13 CANER, M., YIFTAH, S., IA-1276 (1973)

14 CANER, M., YIFTAH, S., IA-1275 (1973)

15 SMITH, J.R., GRIMESEY, R.A., IN-1182 (1969)

16 HINKELMANN, B., KFK 1186 (1970)

17 PRINCE, A., BNL 50168 (1969)

86080034

Appendix 2

Review Papers Presented at the Meeting

A1 S. Raman:

General Survey of Applications which require Actinide Nuclear Data.

A2 J.Y. Barré, J. Bouchard:

Importance des Donnees Nucleaires des Transactinides pour la Physique des Coeurs de Reacteurs Rapides et Thermiques.

A3 H. Küsters, M. Lalović:

Transactinium Isotope Build-up and Decay in Reactor Fuel and Related Sensitivities to Cross Section Changes.

A4 R.M. Nunn:

The Requirements for Transactinide Nuclear Data for the Design and Operation of Nuclear Power Plants.

A5 R.F. Burstall:

Importance of Transactinide Nuclear Data for Fuel Handling.

A6 L. Koch:

Survey of TND Application; European Programs in Waste Management (Incineration).

A7 S. Raman:

Some Activities in the US Concerning the Physics Aspects of Actinide Waste Recycling.

A8 R. Dierckx:

Importance of TND for Fuel Analysis.

A9 A.H.W. Aten:

TND Applications in Radiation and Energy Sources, Tracer Techniques, Life Science, Agriculture and Industry.

86080035

B1 R.W. Benjamin:

Status of measured Neutron Cross Sections of Actinides for Thermal Reactors.

B1/ Contrib. L.W. Weston:

Neutron Capture Cross Sections of the Actinides.

B2 G.D. James:

Status of Neutron Cross Sections of Actinides in the Resonance Region - Linear Accelerator Measurements.

B2/ Contrib. J. Blons, C. Mazur:

Measure de σ_γ de ^{243}Am.

B2/ Contrib. S.M. Kalebin:

Total Neutron Cross Section Measurements on $^{241,243}Am$, $^{244,245,246,248}Cm$.

B3 M.S. Moore:

Status of Neutron Cross Sections of Actinides in the Resonance and Fast Energy Regions - Underground Nuclear Explosion Measurements.

B4 S. Igarasi:

Status of Measured Neutron Cross Sections of Actinides in the Fast Region.

B4,B2/ Contrib. Articles from the Soviet Journal of Nuclear Physics on the Measurement of Fission Cross Sections of: Th229, Th230, Pa231, U232, Np237, Pu239, Bk249, Cf249.

B5a S. Yiftah, Y. Gur, M. Caner:

Status of Transactinium Isotope Evaluated Neutron Data in the Energy Range 10^{-3} eV to 15 MeV.

B5a/ Contrib. The Transactinides in the Main Evaluated Neutron Data Files (CCDN).

86080036

B5b J.E. Lynn:

Theoretical Calculation of TND for Evaluation Purposes.

B5b/ Contrib. M. Caner, S. Yiftah:

A Survey of Cross Section Evaluations Methods for Heavy Isotopes.

B6 S.A. Baranov, A.G. Zelenkov, V.M. Kulakov:

The Experimental Investigation of the Alpha Decay of Actinide Isotopes.

B6/ Contrib. List of Compilations and Evaluations of TND.

B7 C.W. Reich:

Status of Beta- and Gamma-Decay and Spontaneous Fission Data from Transactinium Isotopes.

86080037

L-168

SODIUM FLOW VELOCITY MEASUREMENTS BY CORRELATION OF THERMOCOUPLE SIGNALS.

BY

J. Benkert; C. Mika; K.-H. Raes; D. Stegemann
Institut für Kerntechnik
Techn. University of Hannover, Germany

J. E. de Carlos; I. Melches; A. Perez-Navarro;
F. Verdaguer; B. Zurro
Junta de Energia Nuclear, Madrid, Spain

Introduction: Thermocouples are well known sensors for measuring temperatures. Normally the mean value of the thermovoltage is used in order to detect the absolute temperature of a fluid.

But there is more information in the signal! The turbulent behavior of a fluid generates temperature fluctuations which are registered by thermocouples. The idea is now to use this information in order to derive the fluid-flow-velocity. For this determination two thermocouples with a given distance are being used.

The basic principle is to measure the transit time of the temperature-fluctuations from the first to the second thermocouple. The ratio of the thermocouple-distance to the transit-time gives directly the fluid-flow-velocity (1,2,3).

Although this method looks quite easy, there are a couple of conditions, which have to be taken into account for practical application.

Paper presented at the Specialist Meeting of the IAEA Working Group on NPPCI

Risley, Great Britain, January 1976

86080038

One aim of the extensive investigations is to develope a simple equipment consisting of only two thermocouples and a special correlator with digital output calibrated in [m/s].

Principle of method. The principle, which is being applied to measure the fluid-flow-velocity, is explained in FIG.1. At least two equivalent thermocouples with accurately known distance Δz are placed into the fluid. The temperature fluctuations due to heat transfer from the walls - indicated in the upper part of FIG.1 - will first induce a signal $\vartheta_1(t)$ in TC1 and will then pass on to TC2 to induce a similar signal $\vartheta_2(t)$. Due to the transport of the temperature fluctuations from TC1 to TC2 the signal $\vartheta_2(t)$ will appear the time τ_o later than $\vartheta_1(t)$. The transit-time τ_o can be found from a so called cross-correlation-analysis. The velocity of information v follows directly from

$$v = \frac{\Delta z}{\tau_o}$$

The cross-correlation analysis is essentially the determination of similarity between the two signals $\vartheta_1(t)$ and $\vartheta_2(t)$ by shifting one against the other. The quantitative results give the cross-correlation function (CCF)

$$CCF(1,2) = \overline{\vartheta_1(t-\tau) \cdot \vartheta_2(t)}$$

For computing the CCF generally three operations are necessary

- delaying one signal by the time τ
- multiplying both signals
- time-averaging the product.

For the highest signal-similarity the CCF shows its maximum. This is the case if the delay time τ is identical to the transit-time τ_o between TC1 and TC2. By this procedure τ_o can be easily determined.

During the passage from the first thermocouple to the second the coolant is in heat-exchange with the surrounding wall (tubes, heated pins etc.). This contact influences the transit-time systematically. Due to this and due to the lack of data

86080039

regarding accuracy, measuring-times, positioning of TC's etc. systematic investigations have been performed mainly with sodium of which some results will be presented here, especially in view of practical application.

Experimental Setup.

For the experimental investigations testsections have been inserted into the multipurpose sodium loop ML1 at the Junta de Energia Nuclear (JEN), Madrid, (4,5).

The three testsections designed and used for the experiments in sodium, are shown schematically in FIG.2.

All sections consist of a tube with soldered el. heaters on the outer surface giving a maximum heat flux of about 30 W/cm^2. Testsection I has an inner diameter of 25 mm and 4 mm thickness of the wall. There are five TM-thermocouples in radial fixed positions with axial distances from 19,3 mm to 360,5 mm.

Testsection III differs from testsection I by a smaller inner diameter (16 mm) and increased wall thickness (10 mm). Furthermore five thermocouples can be moved in radial direction. The axial distances between the thermocouples cover the range from 5,5 mm to 225,5 mm.

In both sections the thermocouples are perpendicular to the flow-direction.

It is possible to insert grids, each with five thermocouples, into testsection II. By this a velocity-profile is measureable without moving thermocouples. There is built in also a calibrated flowmeter in order to compare the correlation method with the flowmeter-results under different conditions. The tops of the thermocouples are parallel to the flow direction.

In order to get negligible influences of different transfer functions of thermocouples they have to be equal (6).

A multi-channel-system has been used during the investigations as shown in FIG.3. The DC-compensated TC-output signals are transferred to high gain up to 100K, low noise isolation-amplifiers with high common mode rejection (95 db) and electronic filters (low pass 10 Hz-10 KHz, high pass DC-100 Hz) are used.

86080040

The amplified signals can be stored on multichannel analog tapes (Sangamo) and played back or can be directly transferred to the evaluating part. The evaluation can be performed either by on-line correlators (e.g. Hewlett-Packard HP 3721 A) or via ADC's to digital computers (HP 2116 B, NOVA 1200). For on-line analysis and direct digital display of the fluid-flow-velocity a special real time correlator (MESCH-Correlator), to be described below, was also being used.

Sodium flow velocities could be chosen from 0.5 m/s to 10 m/s. The heat flux was variable up to 30 W/cm^2.

Results.

According to the items of the programs the results will now be presented.

The influence of thermocouple distance Δz upon the maximum of the cross-correlation function is shown in FIG.4 for a typical example. In testsection I five TC's have been positioned along the central axis of the tube. The TC's used are made of Chromel-Alumel (CrAl) with 0.5 mm outer diameter and TM-type construction. The CCF's between the TC's are shown. From the maximum the respective transit-time τ_o can be found. Together with Δz, the velocity $v = \Delta z/\tau_o$ can be calculated. The maximum values for the CCF found here decreases with increasing thermocouple-distance. In other words the larger Δz the smaller the similarity.

As result for practical application the distance between the TC's should be small in order to get a sharp maximum. But on the other hand, the distance should not be too small in order to avoid uncertainties due to inaccuracies in Δz.

The degree of correlation between the two stochastic signals $\vartheta_1(t)$ and $\vartheta_2(t)$ can be quantitatively expressed by the correlation coefficient ϱ. If the two signals look identical then : $\varrho = 1$. If there is no correlation at all then : $\varrho = 0$.

The correlation-coefficient decreases exponentially with increasing thermocouple-distance. This is clearly seen from the upp part of FIG.5. The results presented in this figure have been gained from narrow-band-analysis. Here, high and low pass filters have been used. Mid frequency f_M of 30 Hz means, e.g. the break frequencies (3 db-point) of low as well as high pass filter have

86080041

been positioned at 30 Hz.

The correlation coefficient decreases with increasing mid frequency of the narrow-band-analysis.

But the error of velocity determination shows a minimum for a certain thermocouple distance depending on the frequency band used (6) as shown in the lower part of the figure.

The measured results follow closely the inverse of $\sqrt{T}$. So, if velocities have to be measured with an error of less than $\pm$ 1 % generally measuring times around 10 seconds have to be used. Normally measuring times from 1 to 5 seconds seem to be sufficient if TC-distance and analyzing frequency f_M are chosen properly.

In order to demonstrate the ability of the correlation-technique in sodium, results found from measurements in testsection I are presented in FIG.6. The signals of all thermocouple-combinations have been evaluated to derive the fluid-flow-velocity v. A good consistency of all data can be concluded from FIG.7. The fixed TC-position in testsection I allowed solely to determine the central flow velocity.

A velocity profile across the tube was measured by the variable-position TC's of testsection III. The radial velocity distribution evaluated from three TC-combinations is shown in FIG.7. A calculated curve (solid line) is shown for comparison. The larger deviation of some measured points from the theoretical curve close to the walls is due to the effect of heat exchange between wall and fluid.

The knowledge of the velocity profile is of importance if the throughput is to be measured by this technique, because an integration has to be performed over the diameter. If no theoretical velocity distribution is available for a certain geometry this can be measured either by variable TC's, as shown here, or by TC's distributed radially.

Amongst other applications this technique seems also to be well suited for calibration and recalibration of flow-meters under different field conditions. For all this, however, a simple data evaluation technique is of importance.

860800042

On-line velocity determination and display.

In practice one wants to have for on-line velocity measurements a simple electronic device with thermocouple signals as input and a digital output.

This is realized by a transit time correlator. Basing on the polarity correlation the transit-time of the signals is detected. By counting a shift-frequency the velocity can be measured |7|. By taking into consideration the known thermocouple distance the counted shift-frequency an be calibrated in [m/s].

A comparison between velocity measurements done with a calibrated el. mag. flowmeter and a proto-type of the transit-time-correlato took place in testsection II. FIG.8 shows first results. The rot points represent the maximum velocity calculated from the measure mean value of the el. mag. flowmeter. We got the other points by the on-line-measurements with the transit-time-correlator. This values are less than the others due to the heat-exchange-effects between wall and fluid. Basing on a simple theoretical model |8| the absolute factor K of this effect can be precalculated for the given geometry and frequency range.

This measurements are done with broad-band-analysis from 3 Hz up to 300 Hz. Using a high frequent narrow-band-analysis the difference between the flow-velocity and the velocity of information becomes negligible small as shown in FIG. 5.

Conclusions

From the results of the systematic investigations one can see, that for practical applications the correlation method for determination flow velocities in fluids is very well suited.

In order to have the accuracy as good as possible the following main-points have to be taken into consideration

a) The time-behaviour of thermocouples has to be as fast as possible.

b) Both thermocouples have to have the same transfer-function

86080043

c) The distance between the thermocouples has to be chosen by taking into account the accuracy of positioning the TC's and furtheron the foreseen frequency-range of analysis.

d) Normally measuring times between 1 to 5 seconds are sufficient for accuracies of about 1 %.

Acknowledgement.

The research work reported, is a cooperative effort by Institut für Kerntechnik, Technical University, Hannover, Germany, and Junta de Energia Nuclear, Madrid, Spain.

The experiments in sodium have been strongly supported by the International Bureau of Gesellschaft für Kernforschung m.b.H., Karlsruhe. The authors gratefully acknowledge the support given by these institutions.

86080044

References.

(1) RANDALL, R.L.
Transit time flowmeter employing noise analysis technique
AI-AEC-12941 (1970)

(2) MIKA, C.; RAES, K.H.; STEGEMANN, D.
Untersuchungen zur Kühlmittelgeschwindigkeits- und Durchsatzmessung.

(Investigations concerning measurements of fluid-flow-velocity and throughput)
Tagungsbericht Reaktortagung, 391-394 (1971)
(Compacts of the German Reactor Conference, 1971)

(3) TERMAAT, K.P.
Fluid flow measurements inside the reactor vessel of the 50 MWe Dodeward nuclear power plant by cross-correlation of thermocouple signals.
Journal of Physics E: Scientific Instuments,
Vol. 3, 589-593 (1970)

(4) OLTRA, F.; BOJARSKY, E.; LEISING, H.
Descripcion general del circuito ML-1
(General description of the Sodium-Loop ML-1)
Energia Nuclear, España, 19, 161-169 (1975)

(5) DE LA TORRE,M.; MARTINEZ, DOMENECH, F.J.; GARCIA, M.V.; DE CELIS, B.
Puesta en marcha y experiencia de funcionamento del circuito de sodio ML-1
(Starting and operating experience of the Sodium-Loop ML-1)
Energia Nuclear, España, 19, 171-180 (1975)

86080045

(6) MIKA, C.
Messungen der Strömungsgeschwindigkeit in beheizten Kühlkanälen aus der Korrelation fluktuierender Temperatursignale.
(Measurements of fluid-flow-velocity in heated cooling channels by correlation of fluctuating temperature signals)
Institut für Kerntechnik
Technische Universität Hannover
Dissertation (1975)

(7) MESCH, F.; DAUCHER, H.H.; FRITSCHE, R.
Geschwindigkeitsmessung mit Korrelationsverfahren
(Speed measurements by correlation methods)
Messtechnik, Vol. 78, No. 7 and 8, p. 152-157 and p. 163-168 (1971)

(8) RAES, K.H.
Modelle für die Übertragungsfunktion der Temperaturfluktuationen in beheizten Strömungen
(Models for transfer functions of temperature fluctuations in heated fluids)
Institut für Kerntechnik
Technische Universität Hannover
Dissertation in preparation

86080046

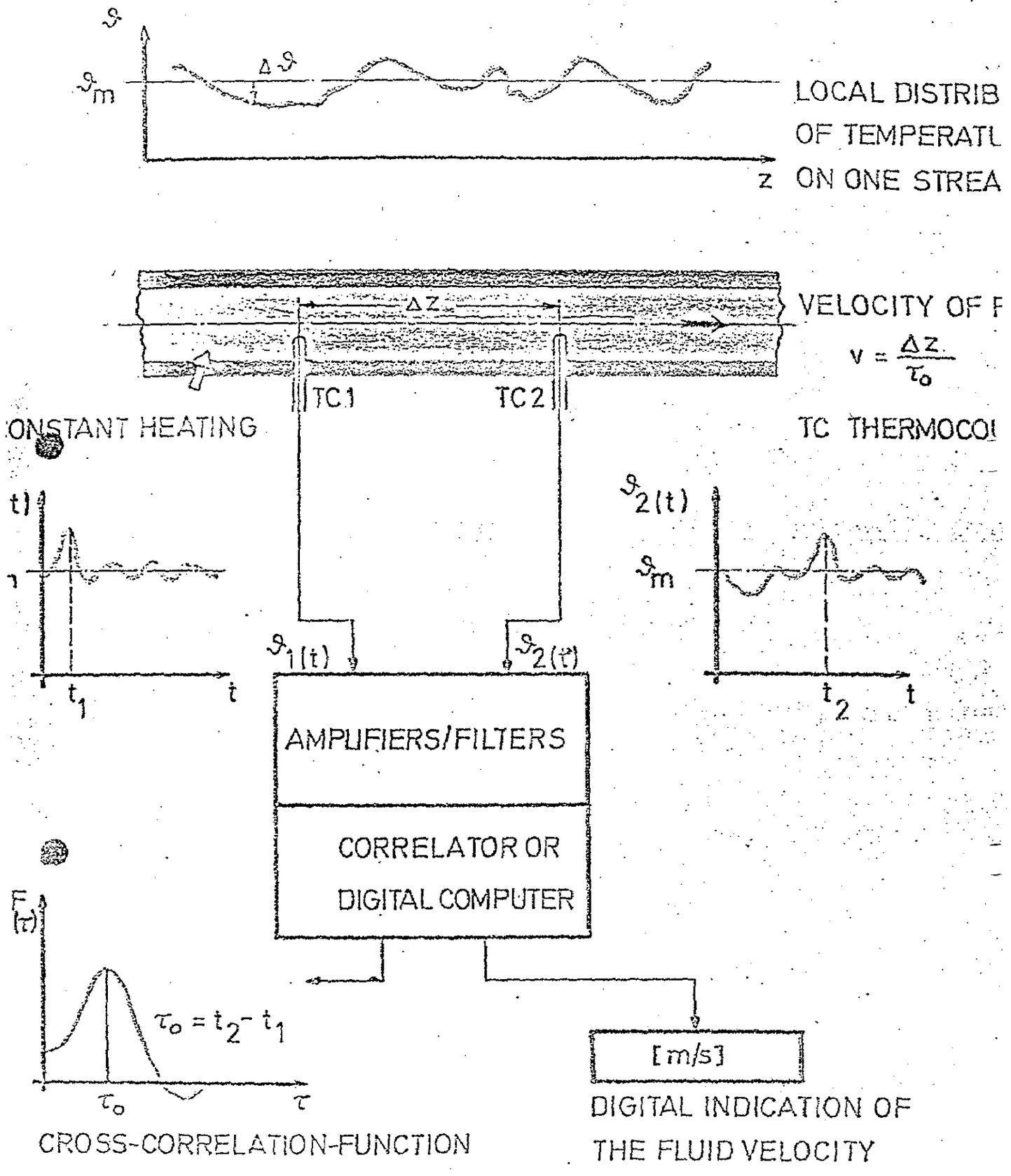

EN/IKH	PRINCIPLE OF METHOD	FIG. 1

86080047

TESTSECTIONS I/III

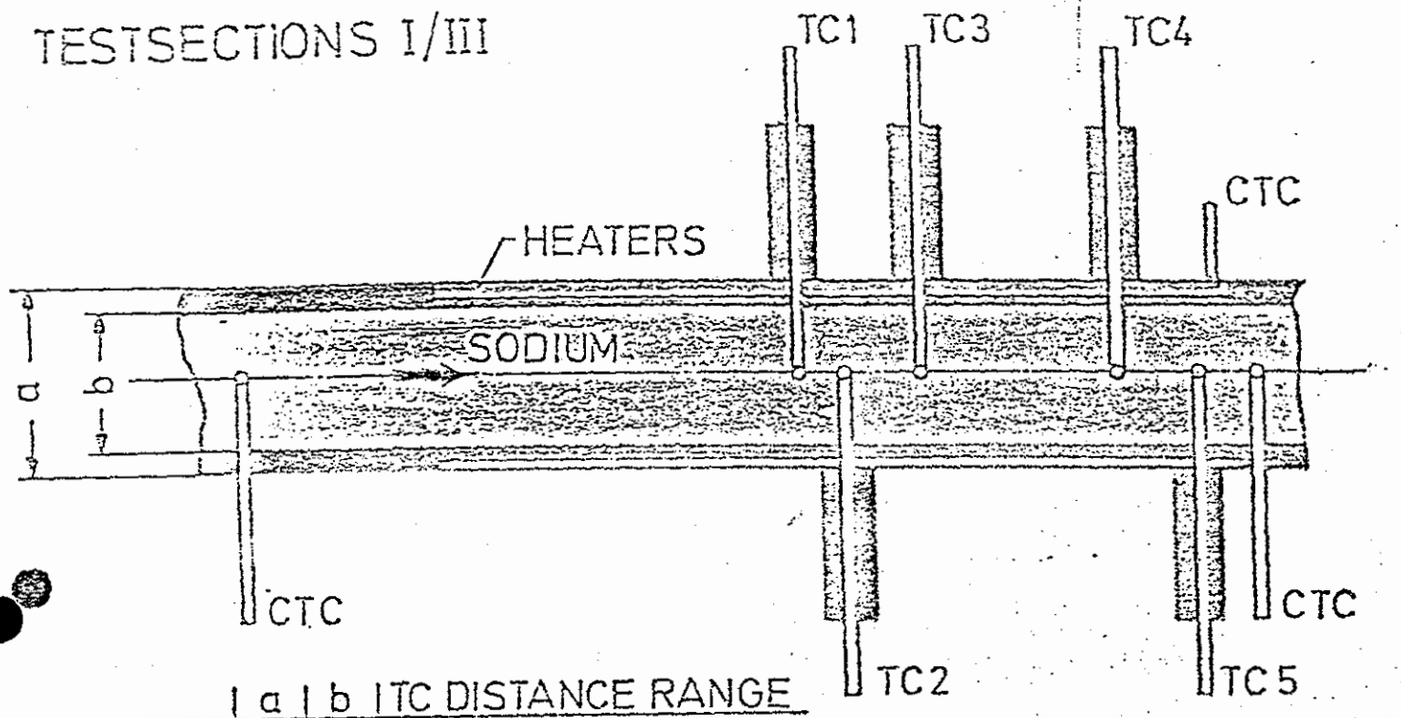

	a	b	TC DISTANCE RANGE
TESTSECTION I	33	25	19.3 TO 360.5 mm
TESTSECTION III	36	16	5.5 TO 225.5 mm

TESTSECTION II

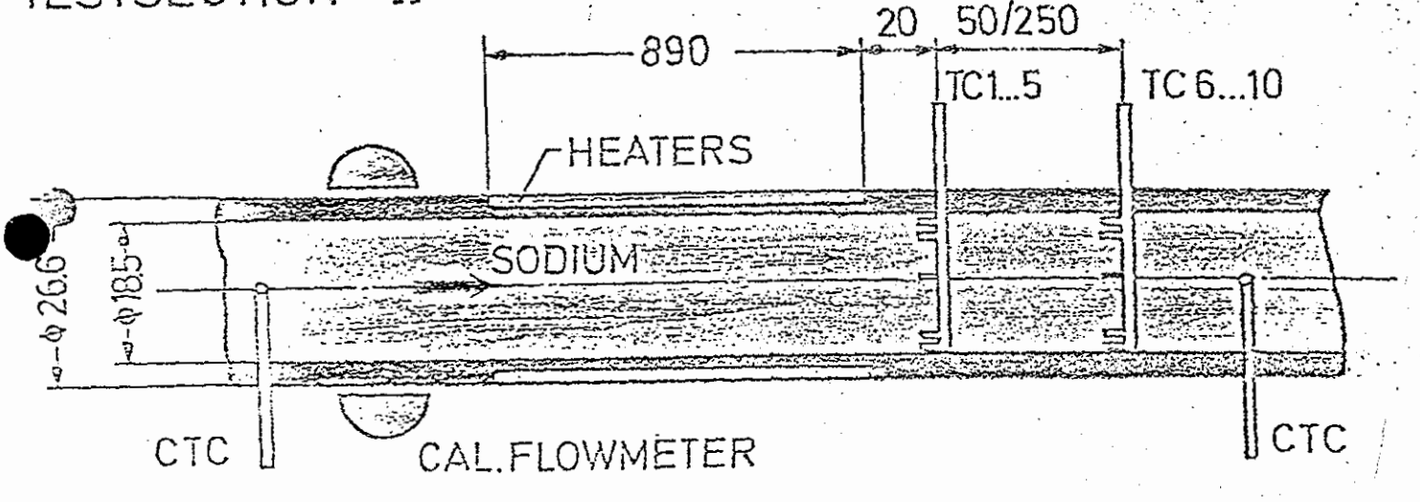

TC THERMOCOUPLE FOR TEMPERATURE FLUCTUATION MEASUREMENTS

CTC THERMOCOUPLE USED FOR SAFETY SYSTEM

JEN/IKH	TESTSECTIONS I. II. III.	FIG. 2

86080048

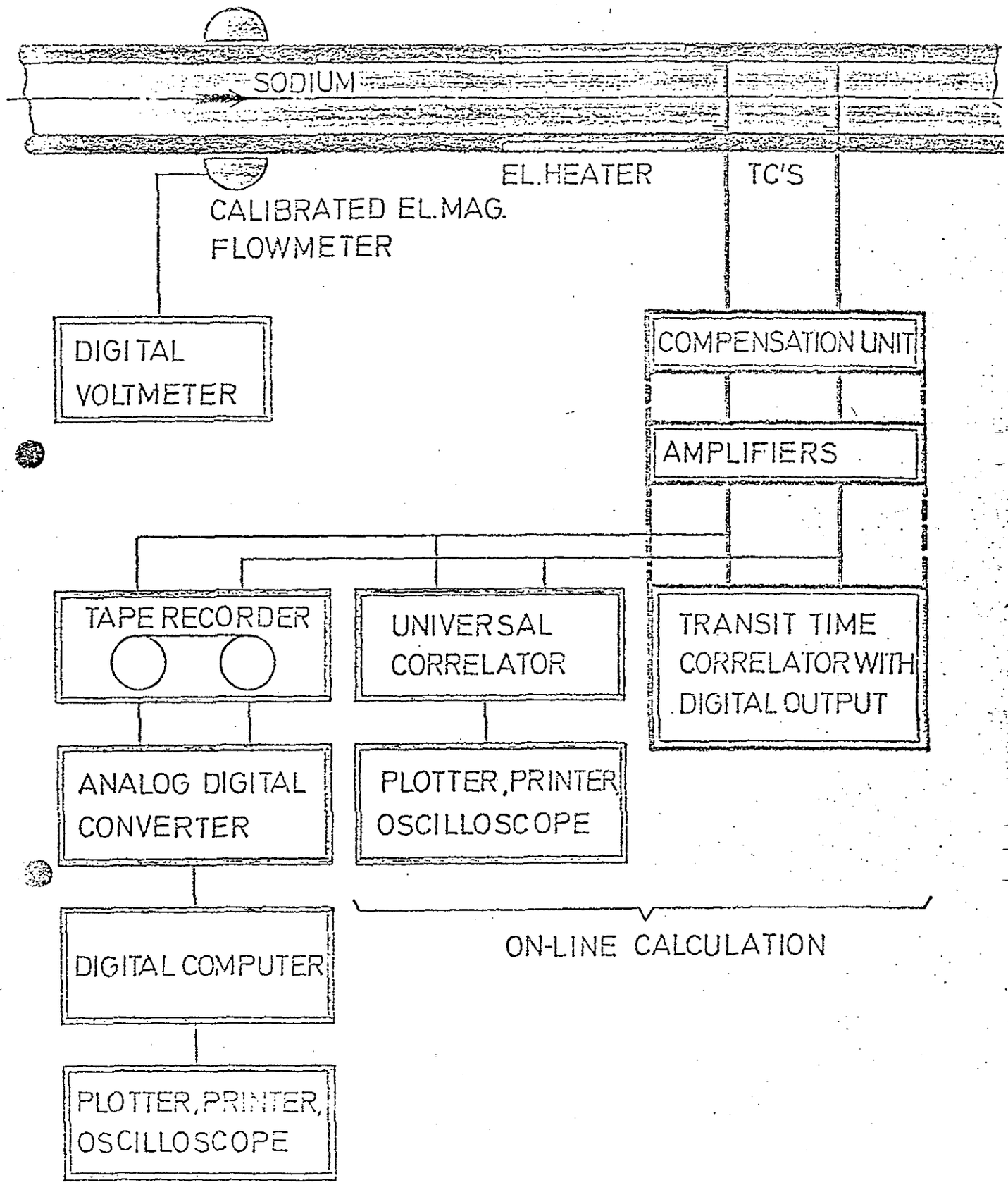

JEN/IKH | EXPERIMENTAL SETUP | FIG. 3

86080049

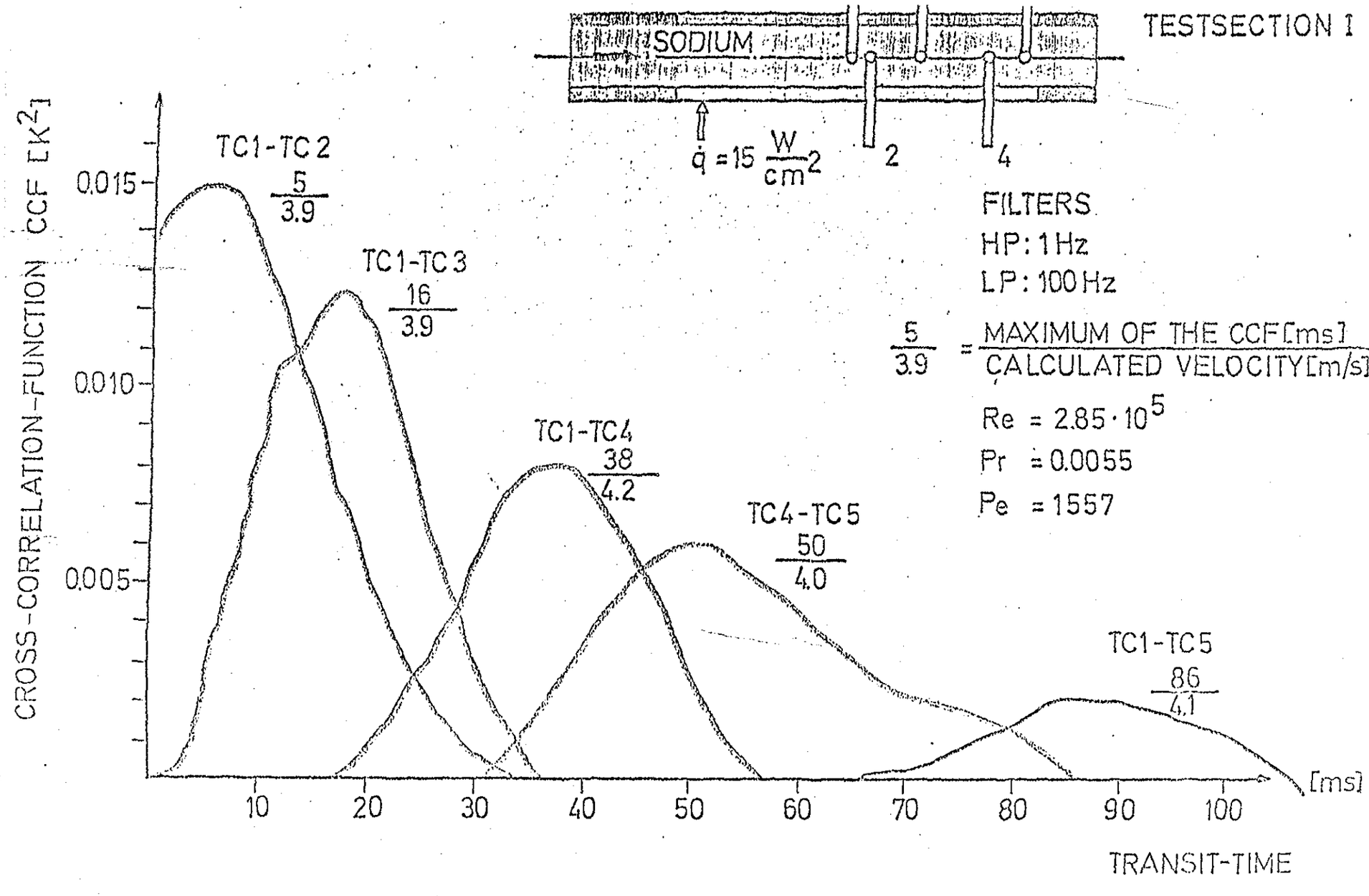

86080050

JEN/IKH

INFLUENCE OF THERMOCOUPLE DISTANCE TO THE CROSS-CORRELATION-FUNCTION

FIG. 4

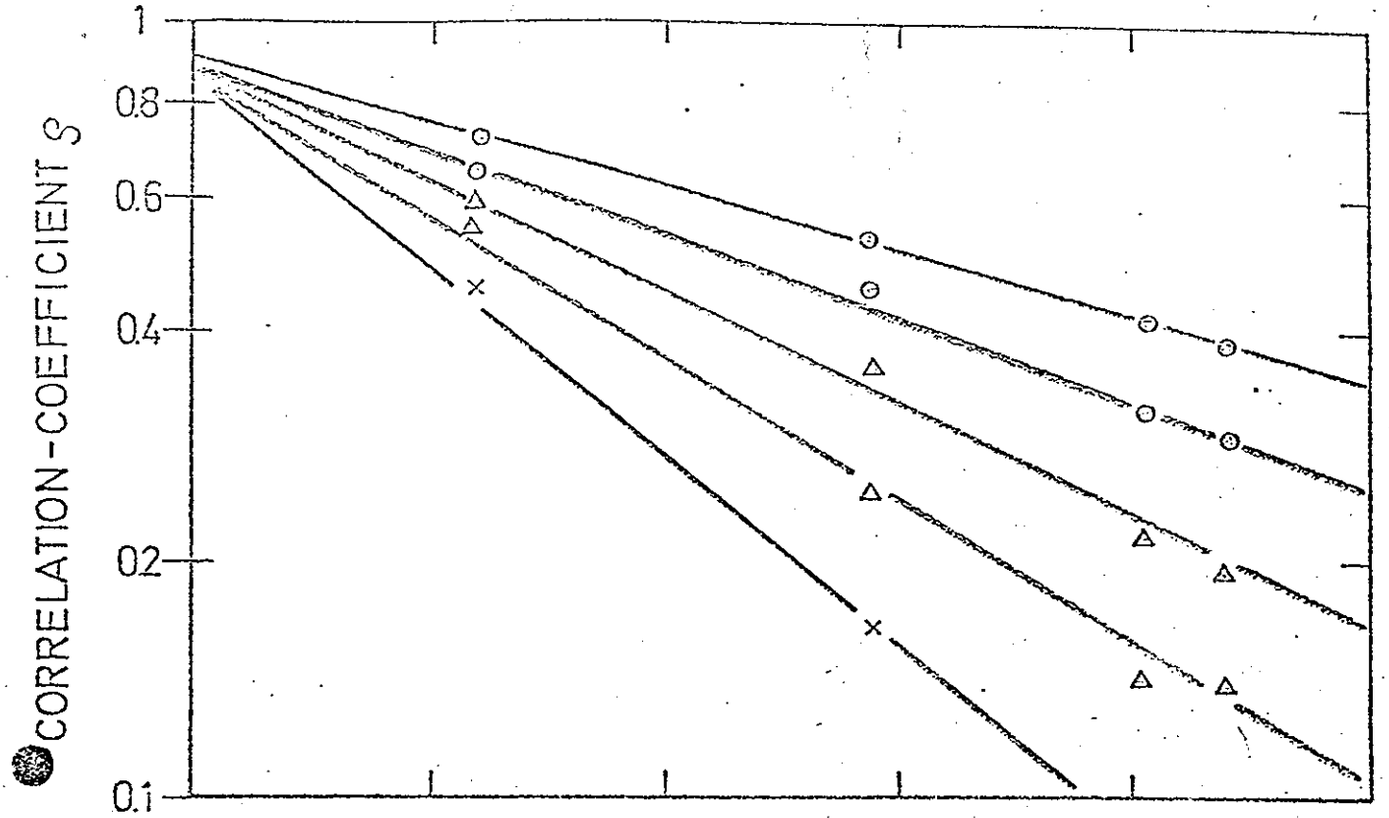

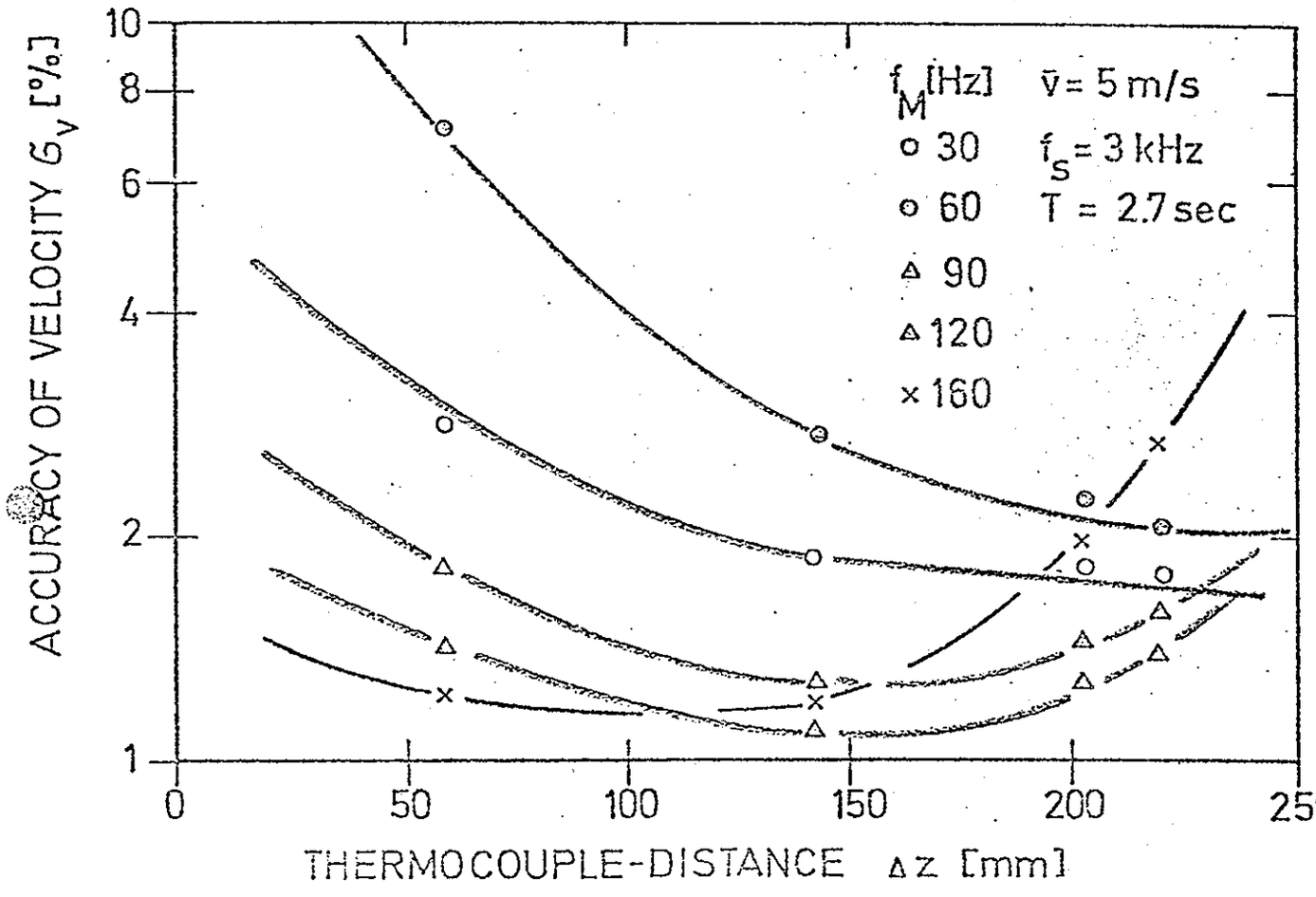

JEN/IKH	ACCURACY OF VELOCITY MEASUREMENTS	FIG. 5

86080051

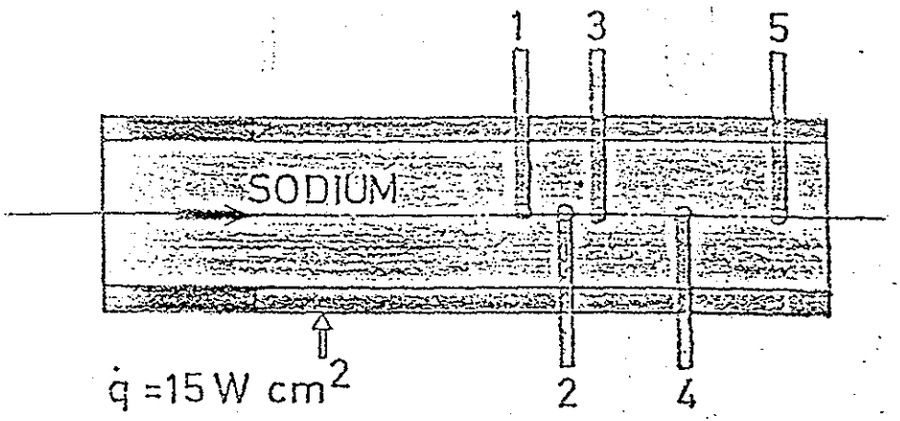

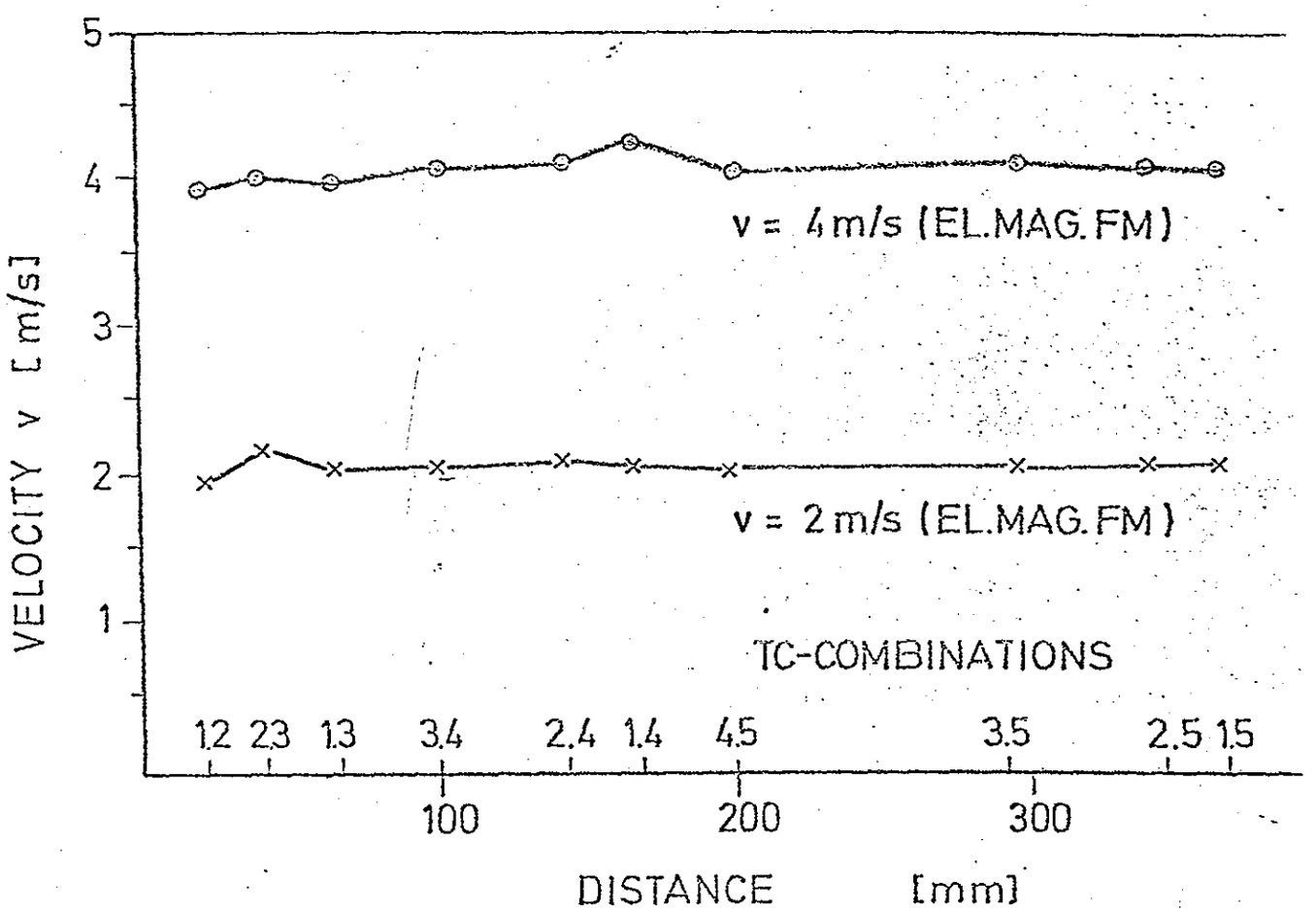

JEN/IKH	MEASUREMENTS OF VELOCITIES IN TESTSECTION I	FIG.

86080052

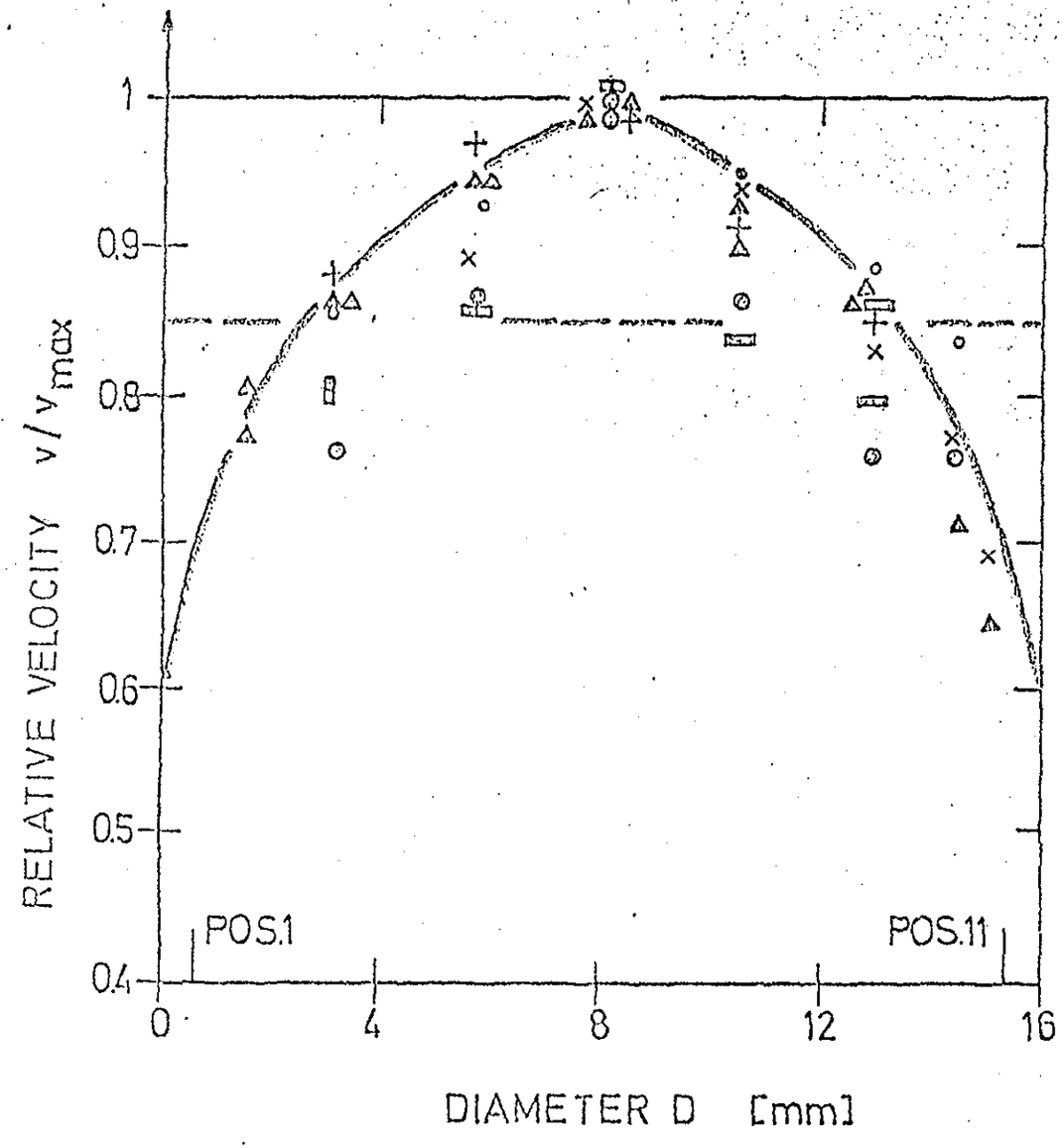

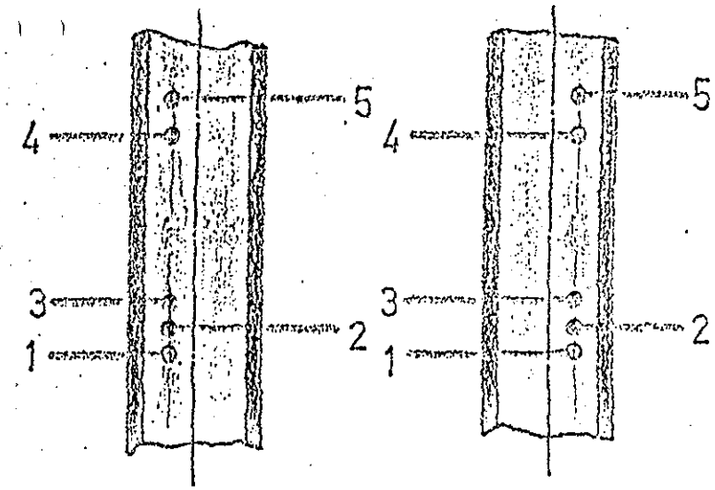

TC-COMBINATION

1/3 ⊙	2/4 △
1/4 ○	2/5 △
1/5 ▭	3/4 ×
2/3 ▭	3/5 +

THEORETICAL PROFILE

MEAN VELOCITY (FM)

$\bar{v}$ = 5 m/s Re = $1.9 \cdot 10^5$

Δf = 1÷100 Hz

JEN/IKH

VELOCITY-PROFILE

FIG. 7

8608005

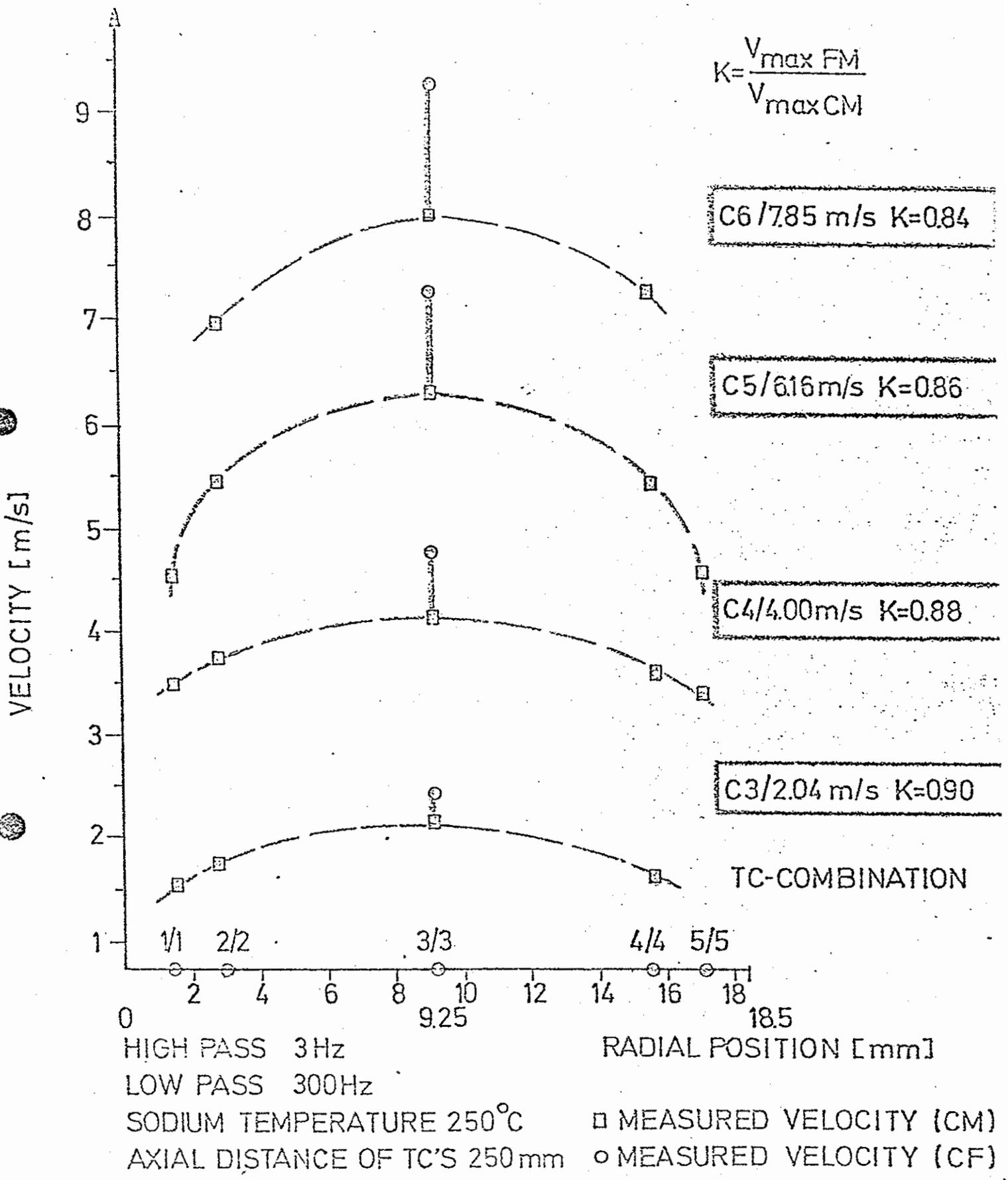

EN/IKH	COMPARISON BETWEEN ○ CALIBRATED FLOWMETER AND □ CORRELATION METHOD	FIG. 8

86080054

Determination of Neutron Spectra and Cross-Section Sensitivity of Tritium Production in a Lithium Sphere

U.Fritscher, F.Kappler, D.Rusch, H.Werle, H.W.Wiese

Kernforschungszentrum Karlsruhe
Institut für Neutronenphysik und Reaktortechnik
7500 Karlsruhe-1, Postfach 3640
Federal Republic of Germany

ABSTRACT

Neutron spectra at several radial positions of a lithium metal sphere with a 14 MeV neutron source at the centre are presented. The spectra are measured both by the time-of-flight method and by proton-recoil detectors. Calculations are performed with the Karlsruhe onedimensional discrete ordinates (S_N) transport code DTK and the neutron cross-section data of the ENDF/B-III data file. The comparison of experimental and calculational results shows good agreement when the measured neutron source spectrum is used in the calculation and when anisotropic elastic scattering is treated carefully. The cross-section sensitivity of tritium production in the sphere was studied by varying the reference cross-section set according to estimated uncertainties in the cross-section of the $^{6}Li(n,\alpha)t$ and $^{7}Li(n,n'\alpha)t$ reactions. The uncertainties in these reaction cross sections yield changes in the tritium production of 0.9% and about 15%, respectively. Finally, the tritium production rate was determined experimentally and is compared with the calculation. A detailed publication of all results is in preparation.

INTRODUCTION

The Karlsruhe lithium sphere experiment has been designed as a set-up of simple geometry and chemical composition and not as a mock-up of a fusion reactor blanket containing lithium, which was published by several authors [1,2,3]. In the case of disagreement of experimental and calculational results for this simple assembly calculations for complex technical fusion reactor blankets should be looked upon very critically.

To check cross sections and calculational models also other one-material experiments were performed: In Jülich HERZING et al. [4] determined the tritium production rate in a cylindrical lithium metal assembly and in Livermore HANSEN et al. [5] measured neutron spectra from materials used in fusion reactors with the exception of lithium.

Our preliminary results, presented at the 8th Symposium on Fusion Technology, 1974 [6], showed large discrepancies and, therefore, further experimental and calculational efforts had to be done.

The effects of cross-section uncertainties of the reactions $^{6}Li(n,\alpha)t$ and $^{7}Li(n,n'\alpha)t$ were studied by varying the reference cross-section set according

86080055

to estimated uncertainties.

Finally, the tritium production rate was determined experimentally and compared with the calculation.

EXPERIMENTS

The assembly is a lithium metal sphere of 1 m diameter coated with a 6 thick shell of stainless steel. Two channels in the equatorial plane, stain less steel tubes each of 60 mm diameter and 1 mm wall thickness, allow by t insertion of appropriate cylinders of lithium metal the measurement of dire tional neutron fluxes at different positions and angles [6] . Through a thi channel the target of a neutron generator is introduced to the centre of th sphere. The source neutrons are produced by a Cockcroft-Walton-type acceler tor for deuterons hitting a tritiated target [6]. The strong space and angl dependence of the neutron spectra is illustrated in fig.1 which shows direc tional neutron spectra measured by the time-of-flight method with two dif ent detectors. A flight path of 10 m was used. The worst energy resolution 15% at 14 MeV, at lower energy e.g. at 1 MeV 11%. In the lower energy regic from 10 keV to 1 MeV a ^{6}Li glass detector, and in the upper energy region 1 250 keV to 14 MeV a NE-213 proton-recoil detector was used. Measurements in side the assembly were performed with small spherical proton-recoil proport al counters. Details of the measurements and their evaluations are given in [6] .

CALCULATIONS

In the calculations the ENDF/B-III nuclear data file [7] and the Karlsruhe onedimensional S_N transport code DTK [8] were used. In this code a special subdivision of the angular region (S_{19}) was prepared in order to take into account the strong anisotropy of the neutron flux which is peaked into the forward direction (0^{o}). For the proper treatment of the highly anisotropic elastic scattering in lithium improved extended transport approximations [9] up to T_5 were used. For a good representation of the neutron source in the energy region from 2 MeV to 15 MeV 55 small energy groups with a lethargy width of 0.03655 were

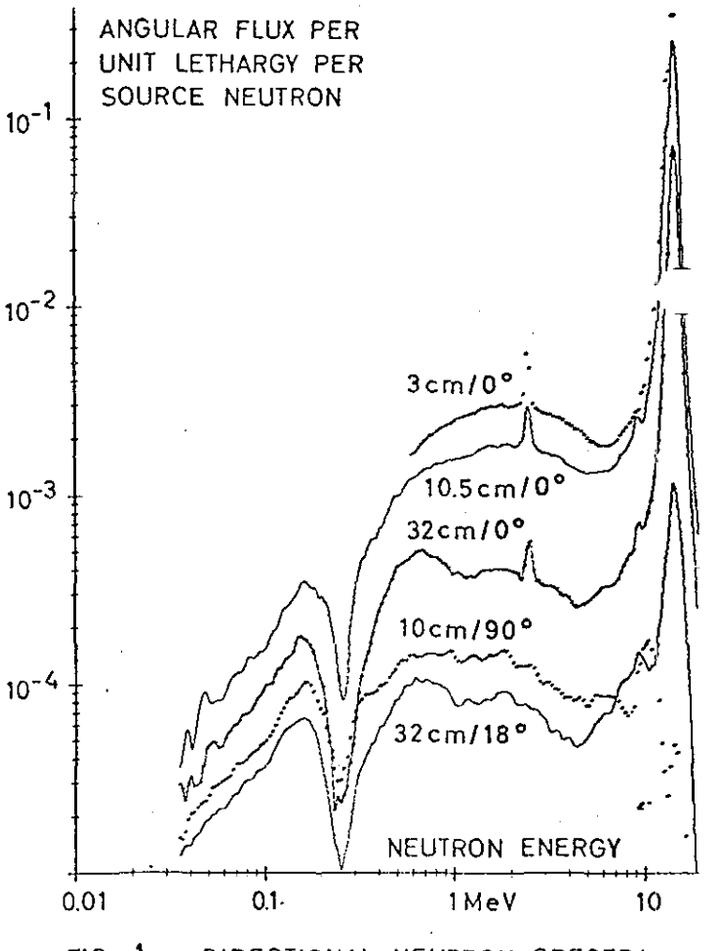

FIG. 1 DIRECTIONAL NEUTRON SPECTRA MEASURED BY THE TIME-OF-FLIGHT METHOD

86080056

chosen. The energy region from 2 MeV to 10 keV was divided into 10 broader groups of different lethargy widths and the energy region below 10 keV was collapsed to one broad group.

The 14 MeV neutrons, which are obtained from the $T(d,n)^4He$ reaction in a tritiated target, are partly slowed down by collisions in the 6.6 mm thick target support. The resulting source spectrum was measured and used in the calculations instead of the monoenergetic 14 MeV neutron source, which was used in the first calculations. Using the experimental source in an empty source region avoids the difficulties of the theoretical treatment of the target zone which might lead to new errors (geometrical representation, materials, inelastic collisions, preequilibrium neutrons). Leakage spectra of 14 MeV neutrons from a 6.6 mm thick iron target support as calculated by the Monte Carlo code KAMCCO [10] and from a 6 mm thick iron shell as calculated by DTK [8] are shown in fig.2. Above 6 MeV there are large discrepancies between measured and calculated neutron source spectra.

The effect of three different source spectra on the neutron spectra inside the lithium sphere is illustrated in fig.3. There are large differences.

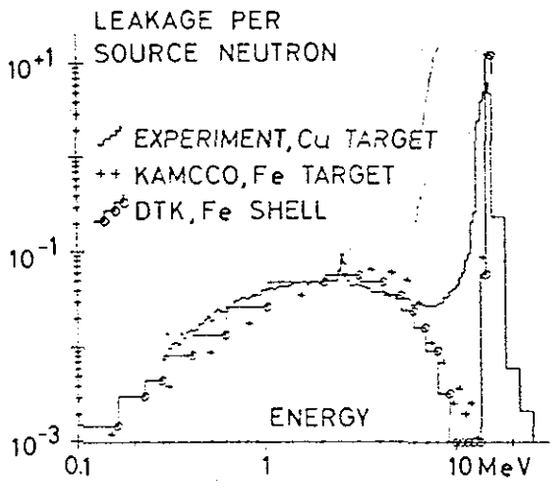

FIG. 2 NEUTRON LEAKAGE FROM THE SOURCE REGION PER UNIT LETHARGY

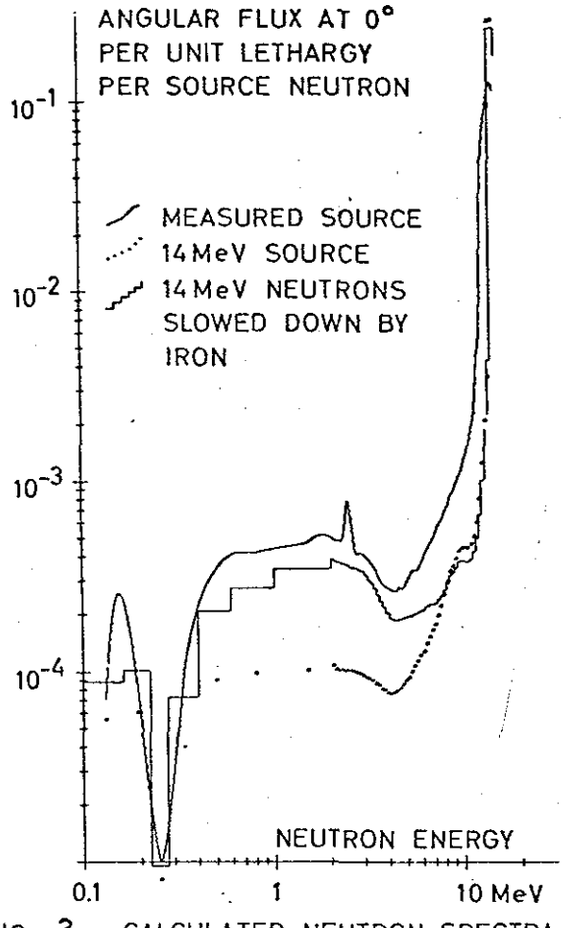

FIG. 3 CALCULATED NEUTRON SPECTRA AT 32 cm / 0°
EFFECT OF DIFFERENT NEUTRON SOURCE SPECTRA

86080057

COMPARISON BETWEEN EXPERIMENT AND CALCULATION

Measured and calculated neutron spectra are compared in the figures 4 . 5. The measured scalar neutron spectra and the directional spectrum at 10.5 cm/0° show relative good agreement with calculation using the normal transport approximation. For a satisfactory calculation of directional neut spectra at a radial distance larger than 10 cm a higher order approximation for the anisotropic elastic scattering [9] must be used to reduce the large discrepancies between measurement and normal transport approximation calcul tion. This is illustrated in fig.5 by the two spectra at r=32cm.

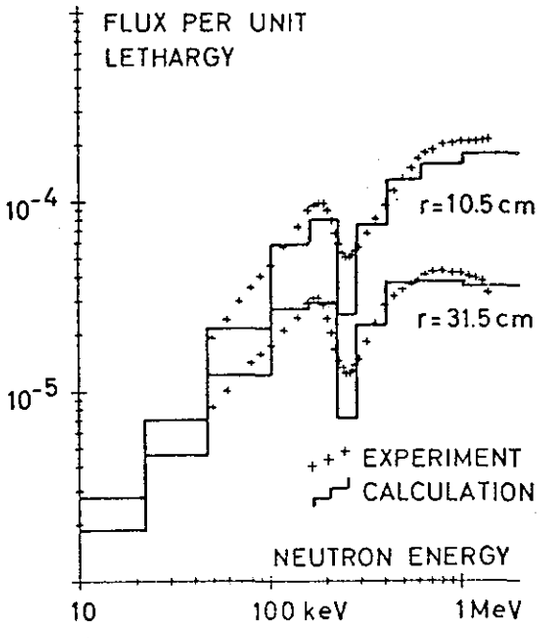

FIG. 4 SCALAR NEUTRON SPECTRA COMPARISON BETWEEN PROTON RECOIL MEASUREMENT AND S_{19} CALCULATION (MEASUREMENT NORMALIZED TO CALCULATION TO EQUAL TOTAL FLUX)

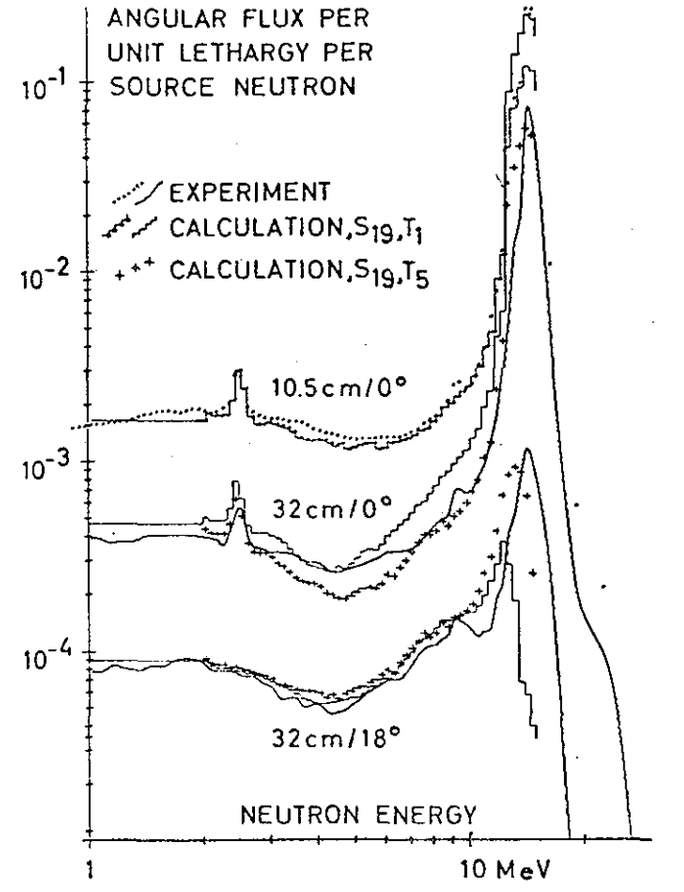

FIG. 5 NEUTRON SPECTRA. COMPARISON BETWEEN EXPERIMENT AND S_{19} CALCULATION: TRANSPORT (T_1) APPROXIMATION AND T_5 APPROXIMATION OF ELASTIC SCATTERING

CROSS-SECTION SENSITIVITY OF TRITIUM PRODUCTION

STEINER and TOBIAS [2] published the cross-section sensitivity of the tritium breeding in a large fusion reactor blanket model. The uncertainties the cross sections of the $^{6}Li(n,\alpha)t$ (0.5% up to 15%) and the $^{7}Li(n,n'\alpha)t$ re tions (20%) attach uncertainties to the tritium-breeding ratio of 0.34% and about 5%, respectively. An analogous sensitivity study using the same uncer tainties for the quoted reaction cross sections resulted in uncertainties c the tritium production rate in the lithium sphere of 0.9% and about 15%, re pectively. This shows that the cross-section sensitivity of tritium product is strongly dependent on the blanket configuration. This dependence is due

860800

the contribution of the reactions $^{6}Li(n,\alpha)t$ and $^{7}Li(n,n'\alpha)t$ to the total tritium production in a blanket. In the lithium sphere the calculated tritium production rate is 0.665 per source neutron which includes 0.550 from ^{7}Li and 0.115 from ^{6}Li. In the fusion reactor blanket studied by STEINER and TOBIAS [2] the corresponding values are 1.4863, 0.5172 and 0.9691. We conclude in accordance with STEINER and TOBIAS [2] as well as with ALSMILLER et al. [3] that the $^{6}Li(n,\alpha)t$ cross-section data appear adequate for calculating the tritium production in a fusion reactor blanket. The uncertainties in the $^{7}Li(n,n'\alpha)t$ cross-section data have to be reduced by a re-evaluation or by new measurements.

TRITIUM PRODUCTION

Following the method proposed by DIERCKX [11] the space dependent tritium production rate in the lithium sphere was determined experimentally by irradiating small Li_2CO_3 probes at several radial positions. Preliminary results are plotted in fig.6 and compared with the calculation. The deviations may have two independent reasons:

1.) Source flux determination in the experiment.

2.) Erroneous cross sections in the calculation.

Final results will be published.

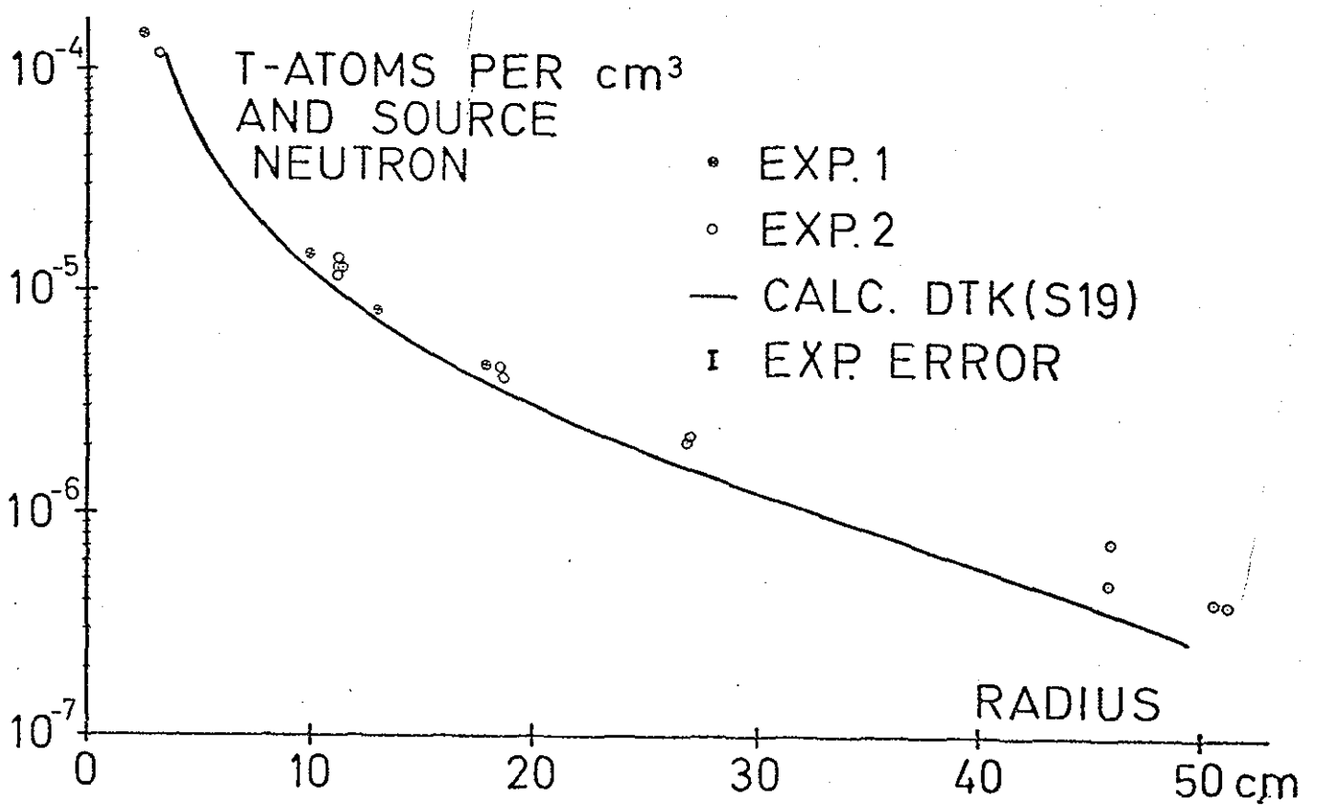

FIG. 6 MEASURED AND CALCULATED TRITIUM PRODUCTION

860800S9

ACKNOWLEDGMENTS

The authors thank J.Braun, Dr.I.Broeders, B.Krieg, E.Stein and D.Woll who made available the ENDF/B-III data set at Karlsruhe and gratefully ackr ledge the help of Dr.C.Günther in preparing the special S_{19} version of DTK.

REFERENCES

[1] DARVAS,J., "Blanket Problems," in "Survey of Fusion Reactor Technolo Euratom Report EUR 4873e, 61 (1972)

[2] STEINER,D., TOBIAS,M.L., "Cross-Section Sensitivity of Tritium Breed in a Fusion Reactor Blanket: Effects of Uncertainties in Cross Sectic of ^{6}Li, ^{7}Li, and ^{93}Nb," ORNL-TM-4200, Oak Ridge National Laboratory (1973) and Nuclear Fusion 14, 153 (1974)

[3] ALSMILLER,R.G.,Jr., SANTORO,R.T., BARISH,J., and GABRIEL,T.A., "Compa rison of the Cross-Section Sensitivity of the Tritium Breeding Ratio Various Fusion-Reactor Blankets," Nucl.Sci.and Eng. 57, 122 (1975)

[4] HERZING,R., KUYPERS,L., CLOTH,P., FILGES,D., HECKER,R., and KIRCH,N., "Experimental and Theoretical Investigations of Tritium Production ir Controlled Thermonuclear Reactor Blanket Model," Nucl.Sci.and Eng. 6C 169 (1976)

[5] HANSEN,L.F., WONG,C., KOMOTO,T.,and ANDERSON,J.D., "Measurements of t Neutron Spectra from Materials Used in Fusion Reactors and Calculatic Using the ENDF/B-III and -IV Neutron Libraries," Nucl.Sci.and Eng. 6C 27 (1976)

[6] KAPPLER,F., RUSCH,D., WERLE,H., WIESE,H.W., "Determination of Neutror Spectra in a Lithium Sphere," Proc. 8th Symp. on Fusion Technology, Noordwijkerhout, The Netherlands,(June 17-21, 1974)

[7] ENDF/201, ENDF/B Summary Documentation, BNL-17541, Brookhaven Nation= Laboratory-report assembled by OZER,O., and GARBER,D. (1973)

[8] GÜNTHER,C., KINNEBROCK,W., "Das eindimensionale Transportprogramm DTK KFK-1381, Karlsruhe (1971)

[9] WIESE,H.W., "Verbesserte Behandlung der Anisotropie der elastischen Neutronenstreuung durch Transportnäherungen energieabhängiger Ordnung Proc. Reaktortagung Nürnberg, Germany, (April 8-11, 1975)

[10] ARNECKE,G., BORGWALDT,H., BRANDL,V., LALOVIC,M., "KAMCCO, ein reaktor physikalischer Monte-Carlo-Neutronentransportcode," KFK-2190, Karlsru (1976)

[11] DIERCKX,R., "Direct Tritium Production Measurement in Irradiated Lithium," Nucl.Instr.and Methods 107, 397-398 (1973).

86080060